INTERNATIONAL GEOPHYSICS SERIES VOLUME 103

OCEAN CIRCULATION & CLIMATE

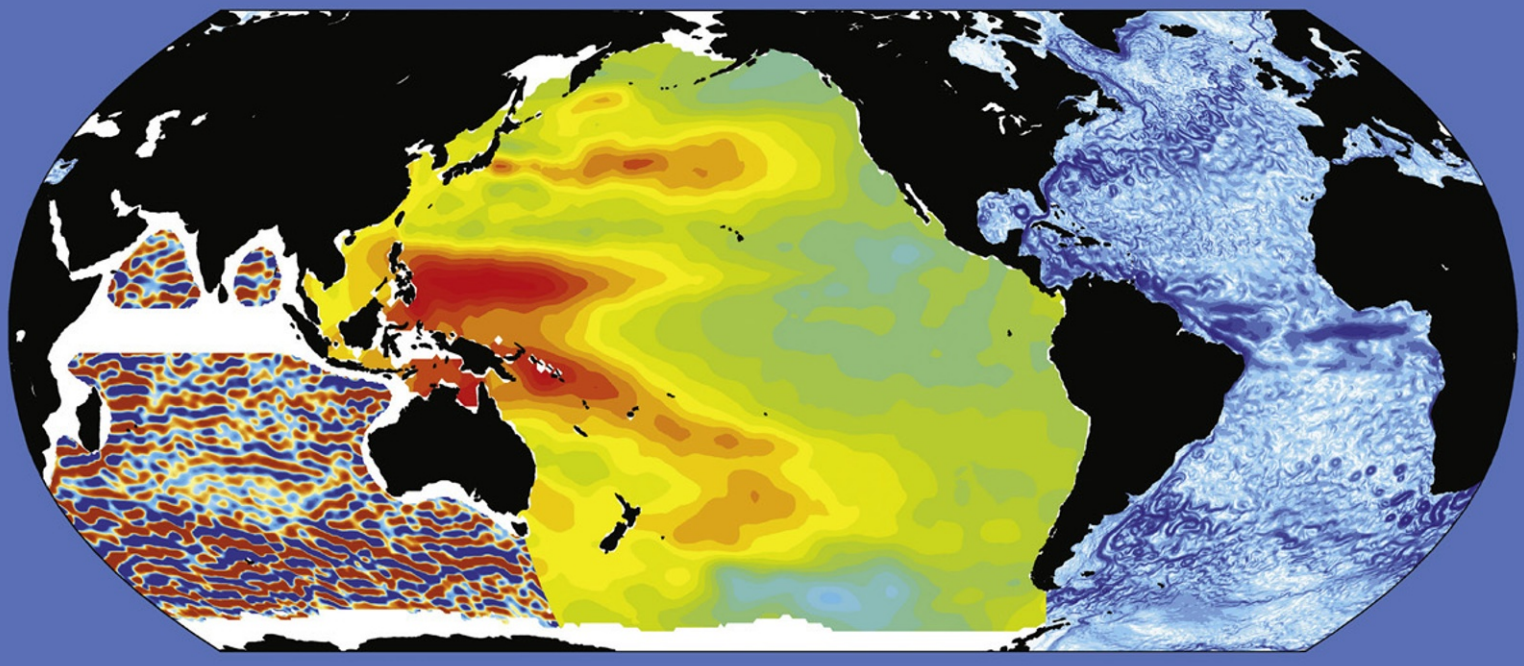

A 21st CENTURY PERSPECTIVE

Edited by
Gerold Siedler, Stephen M. Griffies, John Gould and John A. Church

International Geophysics

Volume 103

Ocean Circulation and Climate

A 21st Century Perspective

Edited by

Gerold Siedler
Helmholtz Centre for Ocean Research
Kiel, Germany

Stephen M. Griffies
NOAA Geophysical Fluid Dynamics Laboratory
Princeton, USA

John Gould
National Oceanography Centre
Southampton, UK

John A. Church
Centre for Australian Weather and Climate Research
A Partnership between CSIRO and the Bureau of
Meteorology, Hobart, Australia

ELSEVIER

AMSTERDAM • BOSTON • HEIDELBERG • LONDON
NEW YORK • OXFORD • PARIS • SAN DIEGO
SAN FRANCISCO • SINGAPORE • SYDNEY • TOKYO
Academic Press is an imprint of Elsevier

Chapter 1

The Ocean as a Component of the Climate System

Thomas F. Stocker
Physics Institute, University of Bern, Bern, Switzerland

Chapter Outline

1. SETTING THE SCENE

From certain points of view, the Earth appears as an almost perfect "aquaplanet" (Figure 1.1). This is a powerful visual testimony to the importance and key role of the ocean in the Earth's climate system. More than 70% of the entire Earth surface is covered by the ocean and therefore most of the lower boundary of the atmosphere is in contact with water or, in the high latitudes, with the seasonal sea ice cover.

The ocean constitutes a virtually unlimited reservoir of water for the atmosphere because it is by many orders of magnitude the largest body of readily accessible water on Earth. Water is the principal resource of all life and thus represents a global commons. A quantitative understanding of the world ocean must therefore be a top priority of Earth System science. Such an understanding rests on three pillars: (i) *in situ* and remote observations with worldwide coverage; (ii) theoretical understanding of processes within the ocean and at its boundaries to other Earth System components; and (iii) capability of simulating ocean and climate processes in the past, present, and future, using a hierarchy of physical–biogeochemical models. Each of these pillars are considered in Section 2, Sections 3 and 4, and Chapter 2, and Sections 5 and 6, respectively.

Due to its large spatial extent and as the principal water reservoir on Earth, the ocean supplies more than 80% of the water vapor for the atmosphere. When the mean atmospheric temperature is higher, the atmosphere contains more water vapor, which is drawn primarily from the ocean. In times of a colder atmosphere that water is returned to the ocean, or when the climate is significantly colder as during an ice age, a significant amount of water is transferred from the ocean to the large ice sheets on land. The ocean is thus the dominant source of the Earth's most important greenhouse gas, water vapor, which is primarily responsible for increasing the Earth's mean surface temperature by about 33 °C to its present value of about 15 °C. Therefore, the ocean is an essential component for habitability of the Earth.

The climate system can be usefully partitioned into seven *spheres* which are physically coupled through exchange fluxes of energy, momentum, and matter. This is schematically illustrated in Figure 1.2. The notion *sphere* should not suggest that the Earth System components are separate entities, they are intertwined. This is, for example, evident for the *hydrosphere* which is present throughout the Earth System. The ocean as the major part of the Earth's *hydrosphere* interacts with all components of the Earth System. It is also coupled to biogeochemical processes through exchange fluxes of substances such as carbon, nitrogen, and many others. Hence, the Earth System cannot be understood without detailed quantitative knowledge of the ocean, its physical properties and the various processes that determine its status and its response to forcings and perturbations.

The ocean is coupled to the *atmosphere* through exchanges of momentum, heat, water, and many substances such as oxygen, carbon dioxide, and other trace gases, and

Ocean Circulation and Climate, Vol. 103. http://dx.doi.org/10.1016/B978-0-12-391851-2.00001-5

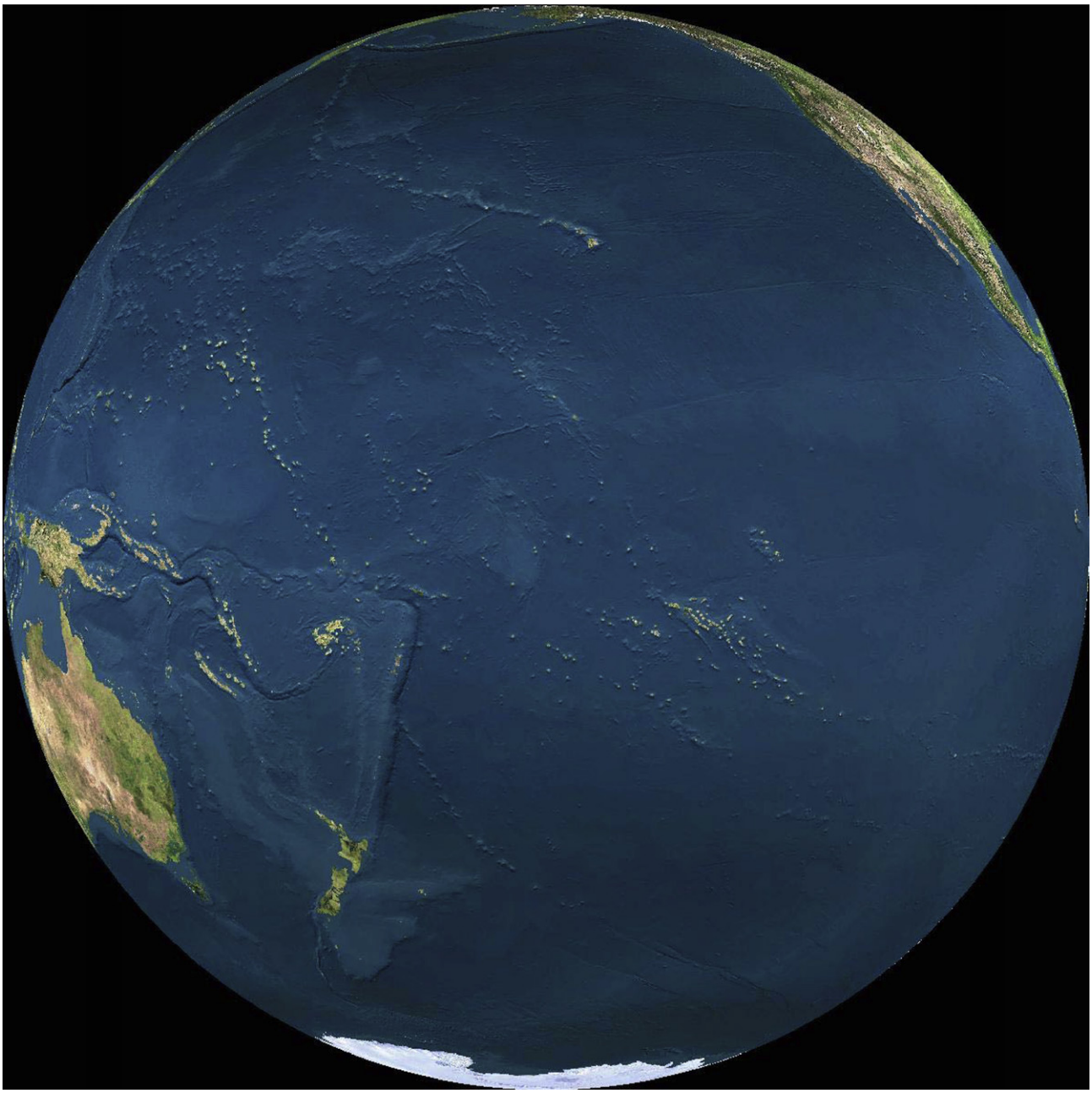

FIGURE 1.1 Ocean appearance of the Earth in an idealized cloud-free view constructed using Earth viewer (from 35,785 km above 10°S, 160°W).

minerals in the form of dust and suspended solids. The exchange of momentum, mediated by the action of wind systems, is the primary driver of the ocean circulation, but also fluxes of heat and freshwater, which influence the density of ocean water and its regional distribution, are important in determining the properties and the flow of water masses.

The *cryosphere* comprises the terrestrial ice sheets, glaciers, and sea ice, and these interact with the ocean directly and indirectly, both through the freshwater supply to the ocean and its effect on sea level (Chapter 27), and through the modification of the ocean–atmosphere heat exchange in the case of sea ice cover (Chapter 16). The ocean is also influenced by the terrestrial and marine *biosphere*, mainly through biogeochemical coupling via fluxes of carbon, oxygen, and nutrients. The *pedosphere*, that is, the land surface, directs river runoff and therefore the spatial distribution of freshwater delivery to the ocean, which modifies water mass properties and ocean circulation. The *lithosphere* comprises the solid Earth which supplies minerals through, for example, volcanism and weathering, and is responsible for processes that

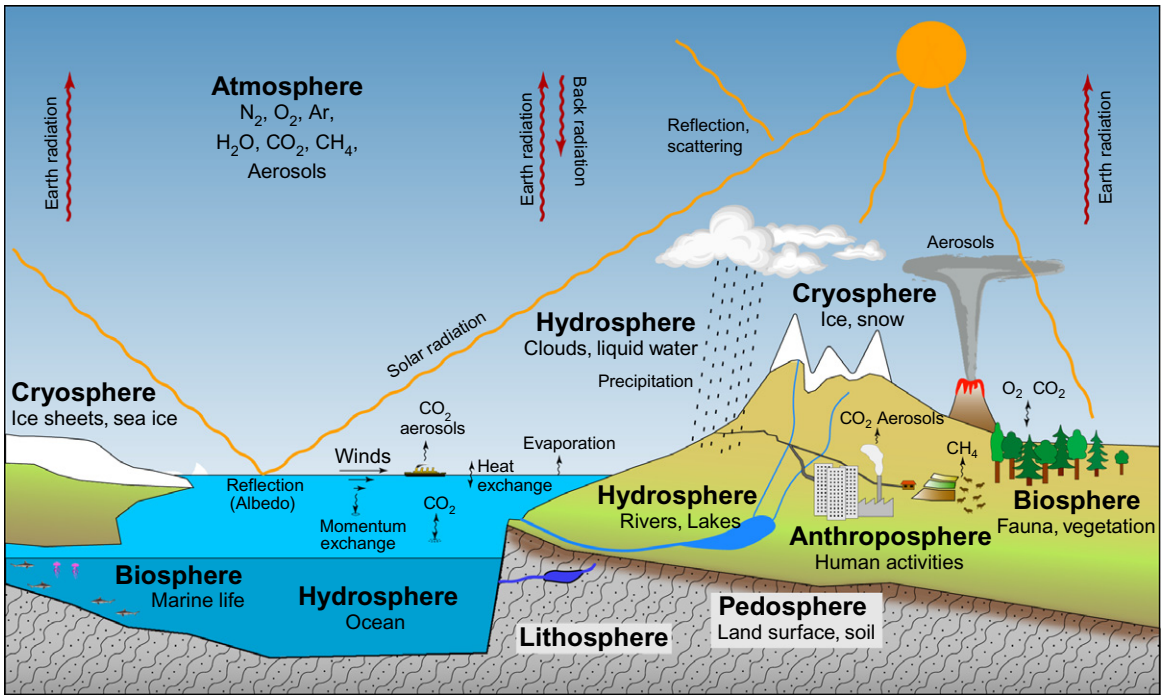

FIGURE 1.2 Illustration of the seven *spheres* of the Earth System, which are intertwined and physically coupled through exchange fluxes of energy, momentum, and matter, and biogeochemically coupled through fluxes of carbon and other substances.

influence the geochemistry of the climate system. It is a component that is relevant when Earth System processes on time scales of 10^5 years and longer are studied.

The latter part of the eighteenth century marks the beginning of the industrial use of coal, and therefore a seventh *sphere* has started to become important in the Earth System. It is the *anthroposphere*, indicated in Figure 1.2, which comprises all human activities, for example, emissions of greenhouse gases through the burning of fossil fuels, land use change, particularly deforestation, and the input of dust and chemical constituents into the various spheres. Further, anthropogenic land surface changes also impact physical properties such as *albedo*, surface roughness, and regional water and heat balances. Human activities have become important drivers of climate and environmental change, and we now live in an epoch in which we leave traces and imprints that will be detectable by our successors using today's classical analytical methods many centuries and millennia from now. It is thus appropriate to put this epoch into a longer-term context of geological epochs by naming it *Anthropocene*, as proposed by Crutzen and Stoermer (2000). Therefore, understanding of the *anthroposphere* and its influence on all the other Earth System spheres is an important prerequisite for assessing the future evolution of the Earth's spheres on a human time scale and thereby for a responsible stewardship of our only home.

2. THE OCEAN AS AN EXCHANGING EARTH SYSTEM RESERVOIR

The ocean covers about 71% of the Earth surface and has a mean depth of 3734 m (Talley et al., 2011) as estimated from the most recent geodetic data analysis (Becker et al., 2009). The ocean volume is about 1.34×10^{18} m^3 and thus contains more than 95% of the Earth's water that participates in the hydrological cycle. In addition, the ocean is a large reservoir of heat, and many substances that are cycled in the Earth System. Particularly, the ocean is the largest storage of carbon, apart from the lithosphere, which is not considered here.

The ocean is a large reservoir of heat with a strong seasonal cycle of temperature observed in the upper 250 m. In the northern and southern hemispheres, the peak-to-peak variations, that is, summer minus winter, of the heat content in the upper 250 m are about 1.4×10^{23} and 2×10^{23} J, respectively (Antonov et al., 2004). The seasonal heat fluxes of 9–13 PW (1 PW $= 10^{15}$ W) which effect these variations are mainly atmosphere–ocean heat fluxes, whereas the net meridional heat fluxes in the ocean are an order of magnitude smaller (see Section 3). The hemispheric asymmetry leads to a net seasonal cycle of the world ocean heat content with an amplitude of about 4×10^{22} J, which peaks in April and assumes a minimum in September

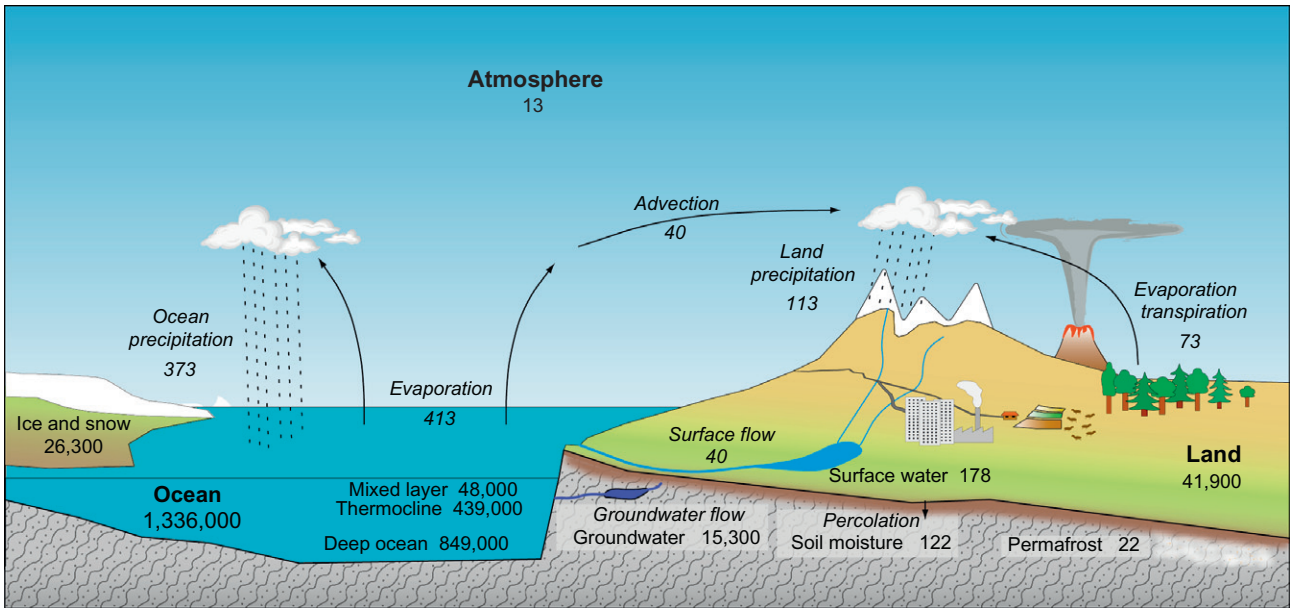

FIGURE 1.3 Inventories of water (in 10^{15} kg) and water fluxes (*italics*, in 10^{15} kg/yr) in the Earth System, based on estimates by Trenberth et al. (2007).

(Antonov et al., 2004; Fasullo and Trenberth, 2008). Seasonal variations of sea-surface temperature are around 2 °C in the tropics and the Southern Ocean, and exceed 10 °C between about 30°N and 50°N in the western parts of the North Atlantic and North Pacific Ocean basins. Together with the seasonal cycle in the wind stress (Risien and Chelton, 2008), this causes substantial changes in the depth of the mixed layer and the thermocline, which in turn determine the upwelling and the availability of nutrients for the marine biosphere.

Observations point to large seasonal variations in the water content of the atmosphere (Trenberth et al., 2007, 2011). Since the ocean is a fundamental component of the global water cycle, seasonal variations must also be present in the freshwater content of the ocean and are expressed most strongly near the surface because of air–sea coupling, continental runoff, and seasonal sea ice export from the polar regions. The summer-minus-winter differences of water content in the atmosphere are about 3×10^{15} kg in the northern, and 1.8×10^{15} kg in the southern hemisphere (Peixoto and Oort, 1992). There are large seasonal variations in the cross-equatorial water flux in the atmosphere, effected by the migration of the Intertropical Convergence Zone. In summer, there is water transport into the northern hemisphere of about 1.8 Sv, while in winter about 1.4 Sv is transported southward. This results in a net northward transfer of water in the atmosphere across the equator of about 0.4 Sv over the course of a year. Consequently, the northern hemisphere experiences an excess of precipitation over evaporation, which is then supplied to the ocean. The ocean closes the global water cycle by a net freshwater transport from the northern to the southern hemisphere of about 0.5 Sv (Wijffels, 2001). This is the net effect of the ocean circulation in all basins, and ocean-based observations are consistent with the estimate of atmospheric freshwater transport, within the uncertainties.

Annual-mean fluxes of water between different reservoirs in the climate system are schematically illustrated in Figure 1.3. They are given as mass fluxes in 10^{15} kg/year. More commonly in oceanography and hydrology, such fluxes are reported as volume fluxes. A widely used and by now standard unit of large-scale volume flux in oceanography is 1 Sv = 1 Sverdrup = 10^6 m^3/s.[1] The large-scale hydrological volume fluxes are more commonly reported in 10^3 km^3/year.[2] Global runoff is thus estimated at about 1.3 Sv (Labat et al., 2004; Trenberth et al., 2007).

Water is transported between the reservoirs by regionally varying evaporation and precipitation, and by transport in the atmosphere and on land (Chapter 5). On a global scale, almost 10 times more water is delivered to the ocean by precipitation than by runoff from the continents. The latter compensates the slight imbalance between evaporation and precipitation over the ocean. The residence

1. This unit was coined by the late Max Dunbar (1914–1995), Professor of Oceanography at McGill University, and is in honor of Harald U. Sverdrup (1888–1957), physical oceanographer, and author of one of the founding treatises in oceanography.
2. Max Dunbar also proposed the volume flux unit Bering, in honor of Vitus Bering (1681–1741), a Danish explorer, who discovered that Asia and America are two separate continents and who charted the west coast of Alaska. The volume flux 1 Be = 1 Bering = 10^3 km^3/yr is a convenient, yet not widely used, large-scale unit in hydrological sciences; 1 Sv ≈ 31.6 Be.

time τ of the water in the world ocean can be estimated by comparing the inventory V with the total influx F to the ocean, that is, $\tau = V/F$. For the ocean, a mean residence time of water is about 3200 years, whereas it is less than 10 days for the atmosphere. However, if one determines the age of a particular water mass in the ocean, the internal transport of water in the ocean, and in particular the vertical transport of water masses, cannot be ignored in this regard. Near-surface waters have a much shorter residence time due to vigorous atmosphere–ocean interaction on a seasonal time scale, for example, the mixed layer has a residence time of somewhat more than 100 years.

In order to appreciate the global significance of the ocean as a reservoir of water, heat, energy, and substances, particularly carbon, inventories, and gross fluxes of some quantities are summarized in Table 1.1. Large uncertainties exist for all quantities, specifically for those associated with the various forms of energy in the ocean (Ferrari and Wunsch, 2009). The total thermal energy of the ocean is about 3×10^{25} J and is given only for the purpose of an order of magnitude estimate of the time it would take for the shortwave radiative input from the Sun to bring a totally ice covered ocean, a condition suggested to have occurred during the "Snowball Earth" phase some 500–1000 million years ago (Pierrehumbert et al., 2011), to today's mean temperature: a surprisingly short time of 6 years (assuming an ice cover of 10 m and all ocean water at freezing point). The energy contained in the general circulation is about 2×10^{25} J (Wunsch and Ferrari, 2004), and therefore of the same order of magnitude, but this quantity is not physically relevant because most of it is potential energy that is not available for the circulation (Ferrari and Wunsch, 2010). The circulation in the ocean is driven by a total supply of energy from the atmosphere of about 2.6×10^{12} W which stems from the input of mechanical energy through the action of wind and from heat fluxes across the ocean surface to compensate for the dissipation of available potential energy (see Table 1.1, footnote h).

The ocean inventories are not constant through time but measurably affected by natural climate variability and anthropogenic climate change (Chapters 27, 28, and 30). The associated anthropogenic fluxes of mass of water, thermal energy, and carbon are also included in Table 1.1. Currently, further mass is added to the world ocean from the melting of the large ice sheets of Greenland and Antarctica, and of ice caps and glaciers around the world. Based on gravimetric satellite data, this amounts to about 3.6×10^{14} kg of water every year. Although only about 1% of global runoff, this additional mass flux constitutes more than 50% of the observed sea-level rise of the past decades, about 1.1 mm/year since 1972 (Church et al., 2011). The world ocean is also absorbing a large amount of thermal energy estimated at a rate of about 1.9×10^{14} W since 1972 (Church et al., 2011), and thus has a slowing effect on anthropogenic climate change, as it stores a substantial fraction of the heat, some of which would otherwise be observed in the atmosphere in response to the increase in greenhouse gas concentrations. This heat causes a warming of the upper ocean and an associated contribution to sea-level rise of about 0.8 mm/year since 1972. A significantly larger average energy flux into the ocean of about $2.3 \cdot 10^{14}$ W from 1993 to 2008 was reported by Lyman et al. (2010).

TABLE 1.1 Estimates of Inventories of Basic Ocean Quantities, Gross Fluxes Across the Ocean Surface, and Anthropogenic Perturbation Fluxes

Quantity	Ocean Inventory	Gross Flux	Anthropogenic Flux
Mass	1.3×10^{21} kg	4.1×10^{17} kg/year	$+3.6 \times 10^{14}$ kg/year[a]
Thermal energy	3×10^{25} J[b]	6×10^{16} W[c]	$+1.9 \times 10^{14}$ W[d]
Kinetic energy	3.8×10^{18} J[e]	1.2×10^{12} W[f]	?
Available potential energy	8×10^{20} J[g]	6×10^{16} W[h]	?
Carbon[i]	38,000 Gt	70 Gt/year	+2.2 Gt/year[j]

Fluxes into the ocean are positive.
[a] *From melting of glaciers and ice sheets from 2003 to 2009 (Riva et al., 2010).*
[b] *Referred to the freezing temperature of sea water (−1.8 °C), and assuming a global mean ocean temperature of 3.8 °C.*
[c] *Annual mean solar energy flux into the ocean (Stephens et al., 2012).*
[d] *From the change in the ocean heat storage from 1972 to 2008 (Church et al., 2011), and later corrected (J. Church, personal communications).*
[e] *Total kinetic energy as estimated by Wunsch (1998).*
[f] *Work done by wind (Munk and Wunsch, 1998).*
[g] *Referred to ocean bottom (Huang, 2010). A smaller estimate of 2×10^{20} J is by Ferrari and Wunsch (2010).*
[h] *Annual mean solar energy flux transferred to the oceans available potential energy. The net flux required to compensate dissipation is much smaller, ca. 1.4×10^{12} W (Oort et al., 1994) from thermal, and 1.2×10^{12} W from mechanical energy flux.*
[i] *In the global mean, 98.8% of dissolved inorganic carbon is in the form of HCO_3^- and CO_3^{2-}. 1 Gt = 10^{12} kg.*
[j] *Estimated mean ocean uptake of carbon 1990–2005 (Denman et al., 2007).*

The world ocean is also a large reservoir of carbon, which exchanges with the atmosphere on a very rapid time scale (Table 1.1, Chapter 30). Ocean carbon is present mainly in the form of dissolved bicarbonate and carbonate whose repartitioning is determined by the ocean's acidity–alkalinity balance. As a carbon reservoir, the ocean is over 60 times larger than the atmosphere and about 16 times larger than the terrestrial biosphere (Denman et al., 2007; Ciais et al., 2013). Carbon is transferred primarily between the atmosphere and the ocean through the gas exchange of CO_2. An associated carbon renewal time is estimated at about 540 years for the entire ocean but significantly faster, only about 13 years, for the carbon found in the surface ocean. The rapid gas exchange and the chemical equilibration between the different dissolved forms of carbon in the surface ocean generate an effective carbon buffering in the world ocean. Therefore, the ocean acts as an important storage of additional carbon from the atmosphere, which results from a variety of human activities, specifically the burning of fossil fuels and deforestation. The increase in the atmospheric carbon inventory, and hence the CO_2 concentration, would be about 70% larger than without the substantial storage effect of the world ocean. In consequence, the ocean plays an increasingly important role as a storage of anthropogenic "waste": the ocean takes up heat driven by changes in the Earth's energy balance, and it takes up carbon due to the increase of CO_2 in the atmosphere.

3. ATMOSPHERE–OCEAN FLUXES AND MERIDIONAL TRANSPORTS

The previous subsection has provided a global overview of the sizes of major inventories and fluxes associated with quantities important for the world ocean. This has merely set the scene, but more relevant information on the role of the ocean in the climate system is obtained from considering the major drivers, in particular their spatial structure at the ocean–atmosphere interface. A large input of mechanical energy is provided by the periodic variations of the differential gravitational attraction between the Earth and the Moon and, to a lesser extent, the Sun, which generate the tides around the globe. Together their supply of power to the ocean is estimated at about 3.5×10^{12} W (Munk and Wunsch, 1998). Tides have a crucial impact on ocean mixing in the interior of the ocean through the breaking of internal waves (Chapters 7 and 8), and dissipation around the continental boundaries and the ocean floor through turbulence, which is generated by the periodic tidal currents. Together with mixing effected by eddies in the mean flow, each with strongly regional patterns, mixing is important on a global scale as it ultimately determines the large-scale aspects of the internal distribution of water masses (Chapters 9 and 10). However, tides have little direct effect on the general circulation of the world ocean, because the tidal residual mean circulation is at least an order of magnitude smaller than the large-scale overturning circulation and smaller still than the large-scale horizontal flow (Bessières et al., 2008).

Instead, the general circulation of the world ocean is mainly driven by the atmosphere–ocean fluxes of three quantities that together supply mechanical, thermal, and available potential energy via the transfer of momentum, heat and freshwater to the ocean (Chapters 11 and 12). The annual mean values of these fluxes and their global distribution are depicted in Figure 1.4.

Momentum is imparted to the surface layers of the ocean through the action of the wind systems in the atmosphere and the associated horizontal stresses on the ocean surface. Surface wind stress is produced by the large-scale atmospheric circulation and partly influenced by air–sea fluxes of heat and water vapor. On a global scale, wind stress is oriented primarily zonally with meridional components that are much weaker. The strongest wind stresses are observed in the westerly wind belt of the Southern Ocean, where they force the Antarctic Circumpolar Current (Figure 1.4a). The wind stress causes most of the large-scale circulation, but only rather indirectly because its effect is strongly modified by the rotation of the Earth. This is achieved by Ekman transport of water over the top few tens of meters of the ocean. Ekman transport scales with the magnitude of the wind stress and is directed to the right (left) in the northern (southern) hemisphere, relative to the wind direction. Its spatial variations cause distortions of the ocean surface and interior layers, which in turn generate horizontal pressure gradients. It is these pressure gradients which drive the large-scale gyre circulations observed in all ocean basins (Chapters 11–14).

The net heat flux to the ocean is a result of the sum of shortwave solar radiative flux, longwave thermal radiative fluxes from the ocean surface (upwelling radiation) and the atmosphere (downwelling radiation), the sensible heat flux, and the latent heat flux. On the global scale, the ocean gains heat roughly between 20°S and 20°N and releases heat poleward of this area. This implies that in the global mean, the ocean must transport heat away from the equator. The world ocean is therefore not simply a passive reservoir but an active component participating in the global heat redistribution in the Earth's climate system (Chapter 29). Regions of strongest heat exchange are clearly identified in the global datasets presented in Figure 1.4b. They are spatially very limited and indicate particular ocean circulation regimes. Heat is taken up in excess of 100 W/m^2 in the eastern equatorial Pacific, where a major ocean upwelling system is located and which generates the most important and coherent mode of internal atmosphere–ocean variability, the El Niño–Southern Oscillation (ENSO) phenomenon. Strong heat release on the order of 150 W/m^2 and more is observed at the western boundaries of the ocean basins, and they coincide

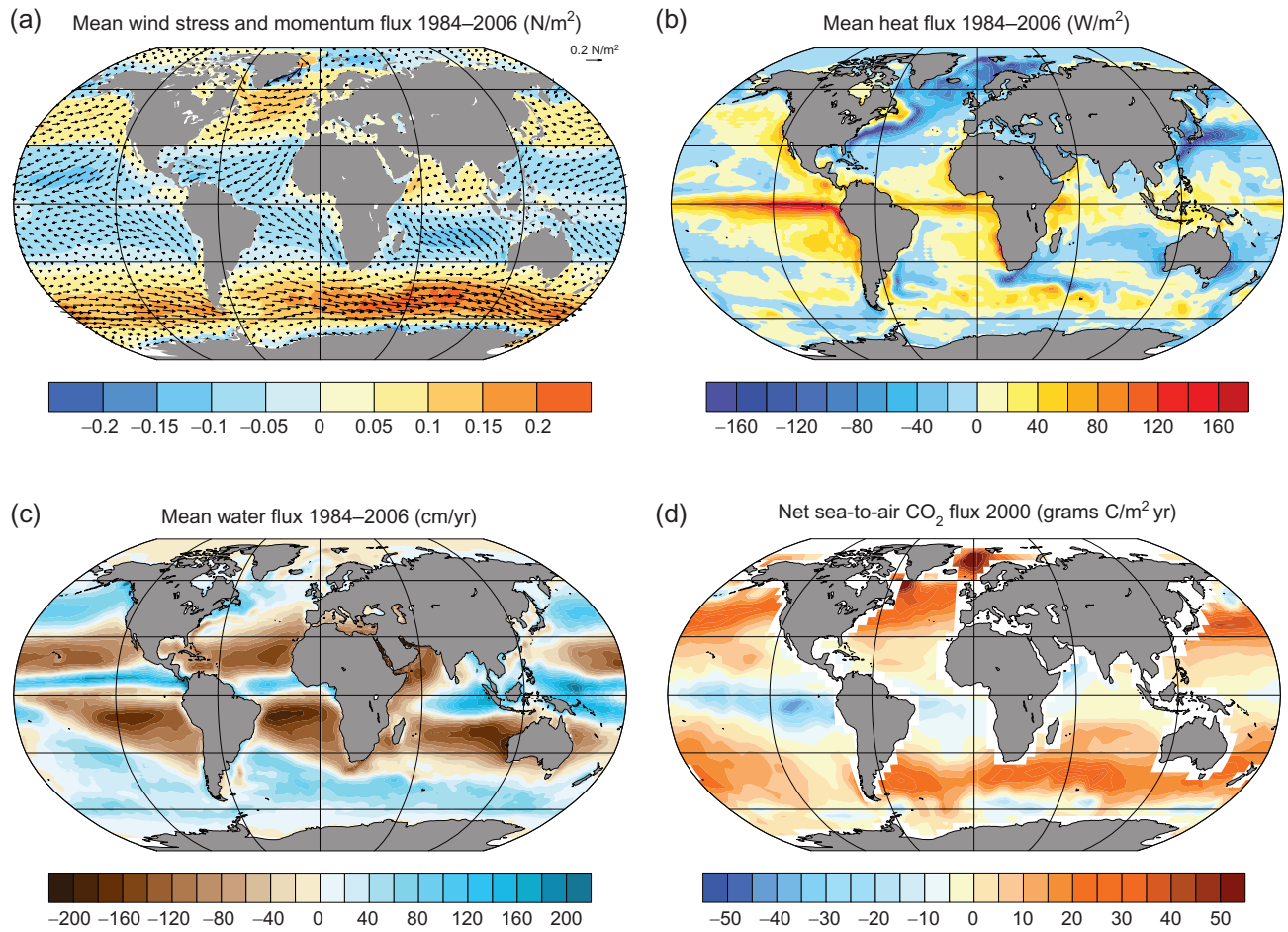

FIGURE 1.4 Major drivers of ocean processes and ocean circulation from various data sources. Shown are time-averaged quantities: (a) wind stress (arrows) and atmosphere-to-ocean momentum flux (colors); (b) net atmosphere-to-ocean heat flux; (c) net freshwater flux excluding river runoff, that is, precipitation minus evaporation, and (d) net atmosphere-to-ocean carbon flux in the year 2000, indicating a large imbalance caused by the uptake of anthropogenic carbon by the ocean. Momentum flux is everywhere into the ocean; positive (negative) values indicate that this flux is caused by a westerly (easterly) wind stress. In panels (b–d), fluxes are positive when they are from the atmosphere to the ocean. *Figures are redrawn based on data from Large and Yeager (2009), and for (d) from Takahashi et al. (2009).*

with the current systems of the Gulf Stream and the Kuroshio, and the Agulhas retroflection off South Africa. Large heat releases are also indicated in the Nordic Seas and the Arctic Ocean. The distinct heat gains and heat losses in the ocean at different latitudes imply meridional heat transports by the ocean circulation in each basin.

The gross flux of freshwater to the ocean is estimated at about 4.1×10^{17} kg/year (Table 1.1) and consists of precipitation (about 90%), river runoff (almost 10%), and ice-sheet melting (nearly 0.1%), the latter being partially compensated by net accumulation on the ice sheets. Imbalances in this freshwater cycle are caused by recent warming and ice-sheet melting. Although they are small (Table 1.1), they are measurable and have a large long-term impact through the rise in sea level. The freshwater balance is achieved mainly by precipitation and evaporation on the ocean's surface, each with a distinct spatial distribution that shows a largely zonal structure on a global scale (Figure 1.4c). This results in a net surface water balance which is characterized by freshwater gain in a narrow equatorial band on the order of 50–100 cm/year with a maximum in the Western Pacific warm pool, freshwater loss to the atmosphere in the subtropical dry zones, and net freshwater gain again in the higher latitudes of both hemispheres. On a global scale, the tropics and subtropics lose freshwater at a rate of about 1 Sv while gains are estimated north of 30°N at about 0.4 Sv, and south of 30°S at about 0.6 Sv (Talley, 2008). As inferred earlier for the heat fluxes, this also implies a meridional transport of freshwater by the ocean circulation in order to close the global water cycle.

A global view of the air-to-sea flux of carbon illustrates the large imprint of the natural carbon cycle at the ocean surface (Figure 1.4d). Carbon enters the ocean in the midlatitudes of the Pacific and Atlantic Oceans roughly in the areas of the Kuroshio and Gulf Stream, and the Nordic Seas. Also, carbon is taken up in a large band circling most of the

Southern Ocean. Major areas of carbon release are located in the tropical Pacific, the Arabian Sea and the northernmost Pacific Ocean, as well as around Antarctica (Takahashi et al., 2009). This latitudinal dependence of air–sea carbon fluxes is mainly temperature driven, as the solubility of CO_2 in warmer ocean water is lower than that in colder water. An imprint of the net uptake of anthropogenic carbon is contained in Figure 1.4d (Chapter 30), but this does not change much the dominant patterns of the gross fluxes.

In the time mean, atmosphere–ocean fluxes are indicators of convergent and divergent meridional fluxes in the ocean. With suitable boundary conditions, for example, no transport across the boundary of Antarctica, meridional fluxes can be calculated from the surface data (Large and Yeager, 2009). This is shown in Figure 1.5. Globally, the ocean transports heat at about 2×10^{15} W northward in the northern hemisphere but only about 0.5×10^{15} W southward in the southern hemisphere. The ocean transports freshwater southward at midlatitudes of the northern hemisphere and, equally, exports large amounts of freshwater from the Southern Ocean. The ocean therefore essentially supplies the freshwater that is lost to the atmosphere in the zones of excessive evaporation (Figure 1.4c). Atmosphere and ocean are therefore tightly coupled through the global water cycle. However, these estimates are plagued with large uncertainties as indicated by directly determined meridional heat fluxes on measurements along hydrographic sections, combined with dynamical constraints as calculated by Ganachaud and Wunsch (2003). They find larger ocean heat transports in the southern hemisphere. Uncertainties are larger still for estimates of the meridional freshwater fluxes in the ocean (Wijffels, 2001).

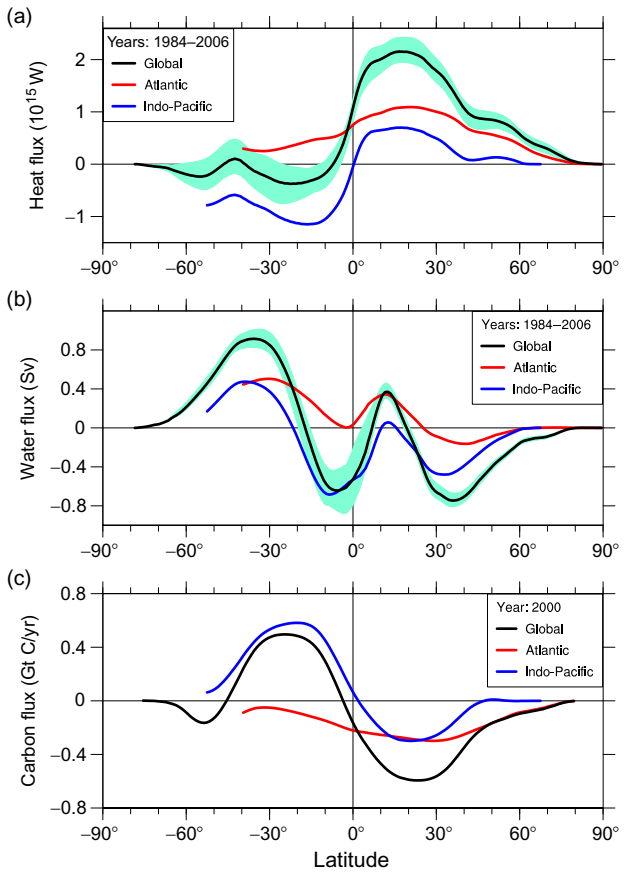

FIGURE 1.5 Global ocean and basin meridional fluxes 1984–2006 of (a) heat, (b) freshwater, and (c) carbon. Meridional fluxes are determined by integrating the data shown in Figure 1.4 in the Atlantic and Indo-Pacific ocean basins from north to south, assuming zero flux at the northern basin boundary and a globally uniform correction for each quantity to ensure zero flux at the southern end. Northward fluxes are positive. The range of interannual variability in global heat and freshwater fluxes is indicated by the turquoise band.

Although uncertainties and differences between the various approaches remain large, a robust picture emerges for the heat and freshwater in the different ocean basins. In the Atlantic ocean, heat is transported northward; in the Pacific and Indian Oceans combined, poleward in both hemispheres. This transport is effected mainly through the meridional overturning circulation (Ganachaud and Wunsch, 2003). The basin-wide meridional heat flux in the Pacific Ocean in the northern hemisphere is northward and carried by shallow overturning, but it amounts to less than half of that carried by the Atlantic Ocean (Talley, 2003).

In terms of freshwater fluxes, various processes need to be considered in addition to evaporation and precipitation over the ocean area: transfer of water from land to the ocean as river runoff, freshwater fluxes between ocean basins through straits, and freshwater transfer from one ocean basin to another via the atmosphere. Global river runoff is estimated at about $1.3\ \text{Sv} \approx 40 \times 10^{15}$ kg/yr (Figure 1.3). Flows through the Bering Strait (about 1 Sv, not considered in Figure 1.5) and the Indonesian Archipelago (about 10 Sv, Chapter 19) connect the Pacific Ocean with the Arctic basin and the Indian Ocean, respectively, and are important elements in the maintenance of the distinctly different salinity signatures of the ocean basins. Further, the Mediterranean Sea, as a marginal basin with an overall excess in evaporation over precipitation, and thus a negative freshwater balance, leaves a large-scale imprint on the salinity distribution of the mid-depth midlatitude North Atlantic Ocean. The global picture of the water cycle would not be complete without taking into account the interbasin transports of freshwater through the atmosphere. The extra-tropical North Atlantic ocean loses about 0.1–0.3 Sv of freshwater through excess evaporation. This water vapor is then carried to the Pacific basin via the trade winds (Zaucker and Broecker, 1992). This is one of the mechanisms to maintain a significantly saltier North Atlantic Ocean (mean salinity of 35.75 at 200 m depth) than the North Pacific (34.50 at 200 m depth) (Levitus et al., 1994).

Meridional fluxes of carbon are depicted in Figure 1.5c estimated from integrating the atmosphere–ocean carbon fluxes of Takahashi et al. (2009). Consistent with Figure 1.4d, carbon is transported toward the equator on

a global scale. In the Atlantic Ocean, carbon is transported southward at all latitudes. Note that these meridional fluxes are based on data from the modern ocean and therefore already contain a significant anthropogenic contribution. For example, under preindustrial conditions, all ocean basins are found to export carbon to the Southern Ocean. This transport has now changed direction in some areas due to the large uptake of anthropogenic carbon in the Southern Ocean (Figure 1.4d).

These large-scale air–sea fluxes and meridional fluxes of heat, freshwater, and substances are the manifestation of the tight coupling between the atmosphere and the ocean. Therefore, data as presented in Figures 1.4 and 1.5 are strong additional constraints for a global view of the ocean circulation.

4. GLOBAL-SCALE SURFACE AND DEEP OCEAN CIRCULATIONS

The global view of atmosphere–ocean fluxes and the implied meridional transports of heat, freshwater and carbon have pointed to the existence of a worldwide ocean current system. Its surface flow is characterized by basin-wide gyre circulations in the Atlantic, Pacific, and Indian Oceans (Chapters 11–14). The near-surface circulation can be divided roughly into five major phenomena: in the northern hemisphere, anticlockwise subpolar gyres (Chapter 17), clockwise subtropical gyres and mainly zonal equatorial current systems (Chapter 15); in the southern hemisphere, the anticlockwise subtropical gyres and the Antarctic Circumpolar Current (Chapter 18). A qualitative, global overview is given in Figure 1.6. For the strong subtropical gyres of the Pacific and Atlantic Oceans, transport estimates are at 42 Sv for the Kuroshio (Imawaki et al., 2001), and 30 Sv through the Strait of Florida (Lumpkin and Speer, 2003); about 134 Sv are carried by the Antarctic Circumpolar Current through the Drake Passage (Cunningham et al., 2003). This information, together with knowledge of the sea-surface temperature distribution, permits a rough estimate of the heat carried by the subtropical gyre in the North Atlantic Ocean. Assuming a volume transport of 30 Sv and a temperature difference of about 2 °C between the northward flowing warm water at the western boundary and colder water whose southward flow is spread over most of the Atlantic basin width east of the western boundary current, we obtain $F_H = \rho \cdot c \cdot \dot{V} \cdot \Delta T \approx 10^3 \times 4 \times 10^3 \times 30 \times 10^6 \times 2\mathrm{W} = 0.24 \times 10^{15}\mathrm{W}$ for the meridional heat flux by the subtropical gyre. However, estimates for the total meridional heat flux in the North Atlantic are about 1.3×10^{15} W (Ganachaud and Wunsch, 2000; Johns et al., 2011). This implies that there must exist another important type of circulation in the Atlantic ocean that carries the missing heat. This is the deep meridional overturning circulation of the Atlantic ocean, referred to as the Atlantic meridional overturning circulation (AMOC).

A global-scale circulation in the deep ocean (Chapter 10) has been suspected since the early days of ocean exploration, when it was realized that even in tropical latitudes, the deep ocean is very cold. Such waters could only be supplied from polar regions where the annual mean temperature is sufficiently cold. This also suggests that the deep waters derive from surface, or near-surface waters, of the high latitudes. The latest comprehensive international effort, in the framework of the World Ocean Circulation Experiment (WOCE, www-pord.ucsd.edu/whp_atlas), has measured the global distributions of temperature, salinity, and many tracers, and produced a comprehensive view of the global water masses and their physical and chemical characteristics. The view of the importance of a globe-encompassing deep circulation in the world ocean has been confirmed in great detail by this immense dataset.

Figure 1.7 shows a representative section through the Atlantic Ocean for temperature and salinity and indicates the three dominant water masses in the Atlantic. The coldest waters in the deep ocean can be traced back to regions around Antarctica where Antarctic Bottom Water (AABW) is formed. North Atlantic Deepwater (NADW) is less dense and hence is located between AABW and Antarctic Intermediate Water (AAIW). The presence and extent of these water masses suggest that deep water is being formed in the high latitudes in rather localized areas. In order to close the flow, the simplest possibility is that water upwells uniformly on a global scale as proposed by Munk (1966). He estimated a global mean upwelling rate of 0.7×10^{-7} m/s using mean vertical structures of temperature, salinity, and radiocarbon, from the central Pacific Ocean. This is consistent with a recent estimate of the global deep water production of 36 Sv which would need to be replenished by a global mean upwelling rate of 10^{-7} m/s (Ganachaud and Wunsch, 2000). Incidentally, this order of magnitude for global upwelling yields a renewal time for the entire ocean volume of about 1000 years, which is significantly faster than the earlier estimate based on Table 1.1. This time is also more consistent with estimates of the age of the oldest waters in the Pacific based on radiocarbon measurements and inverse calculations (Gebbie and Huybers, 2012). However, more detailed observations have uncovered a distinctly regional structure of upwelling, with most of it occurring in the Southern Ocean and equatorial regions (Döös et al., 2012; Marshall and Speer, 2012). In both areas, the upwelling is largely wind-driven by eddy-induced momentum transport and Ekman divergence.

Figure 1.7 also suggests that the deep circulation is essentially a meridional overturning circulation, which is characterized in the Atlantic Ocean by warm waters flowing northward and colder waters at depth flowing southward, each in western boundary currents. This view for the Atlantic Ocean was first proposed by Stommel (1957),

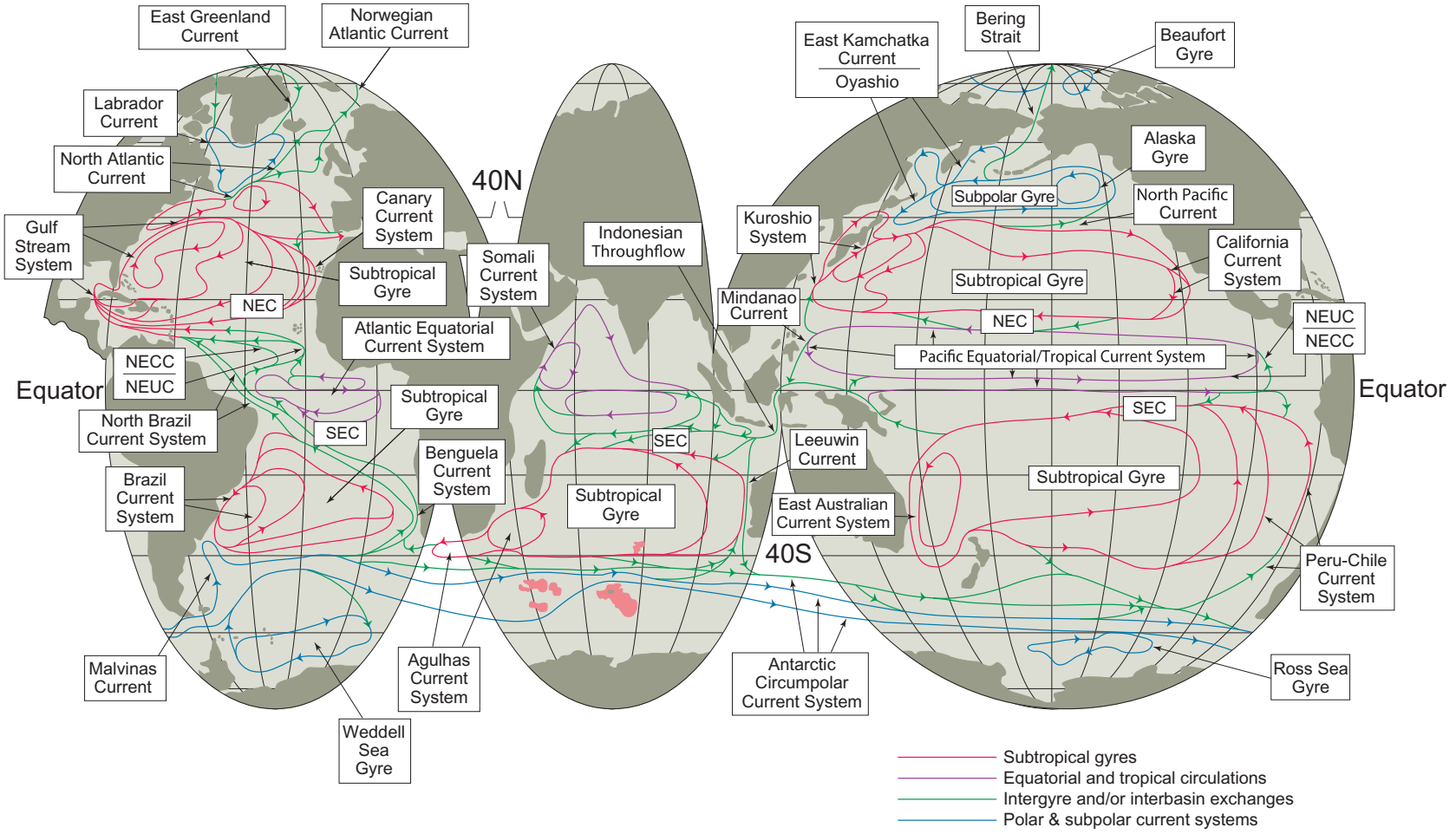

FIGURE 1.6 Illustration of surface circulation systems of the world ocean. NEC and SEC denote the Northern and Southern Equatorial Currents, NEUC and NECC are the Northern Equatorial Under and Counter Currents, respectively. *Figure from Talley et al. (2011), based on an earlier version of Schmitz (1996).*

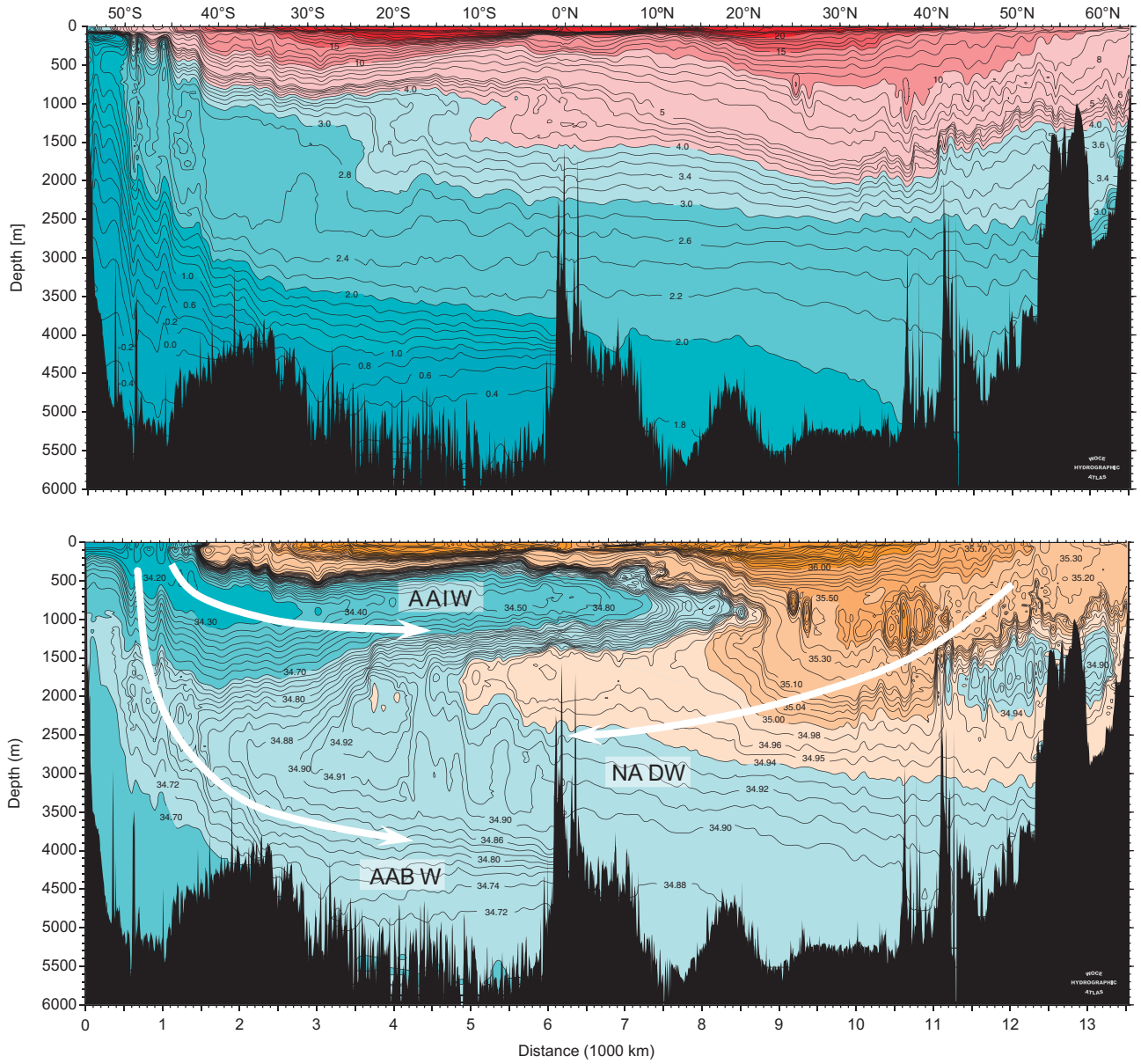

FIGURE 1.7 Distribution of potential temperature (upper panel) and salinity (lower panel) along a section through the Atlantic Ocean from the Southern Ocean to Iceland. The major water masses in this ocean basin are North Atlantic Deep Water (NADW), Antarctic Intermediate Water (AAIW), and Antarctic Bottom Water (AABW). They are characterized by specific ranges of temperature and salinity and thus visible in both quantities. Arrows schematically trace their pathways. *From the WOCE Hydrographic Atlas (Koltermann et al., 2011).*

based purely on dynamical considerations of a fluid on a rotating sphere, but inspired by earlier insight from direct measurements (Defant, 1941). Stommel (1958) extended this concept qualitatively to the entire ocean and provided estimates of the volume transport for each of the deep western boundary currents. It is worth noting that Stommel closed his landmark paper, presenting for the first time a global view of the deep circulation of the world ocean, by saying *One cannot pretend that it describes the abyssal circulation accurately in detail*. The quantitative and dynamically consistent analysis of the deep circulation was presented in a series of papers starting with Stommel and Arons (1960).

Stommel's Letter to the Editors (1958) prompted a series of iconic depictions of the global deep ocean circulation (Richardson, 2008); the most popular is the *Great Ocean Conveyor Belt* (Broecker, 1987b). Broecker and Peng (1982) introduced the term *large conveyor belt* and described the geochemical significance of this global circulation. A schematic illustration that indicates the flow

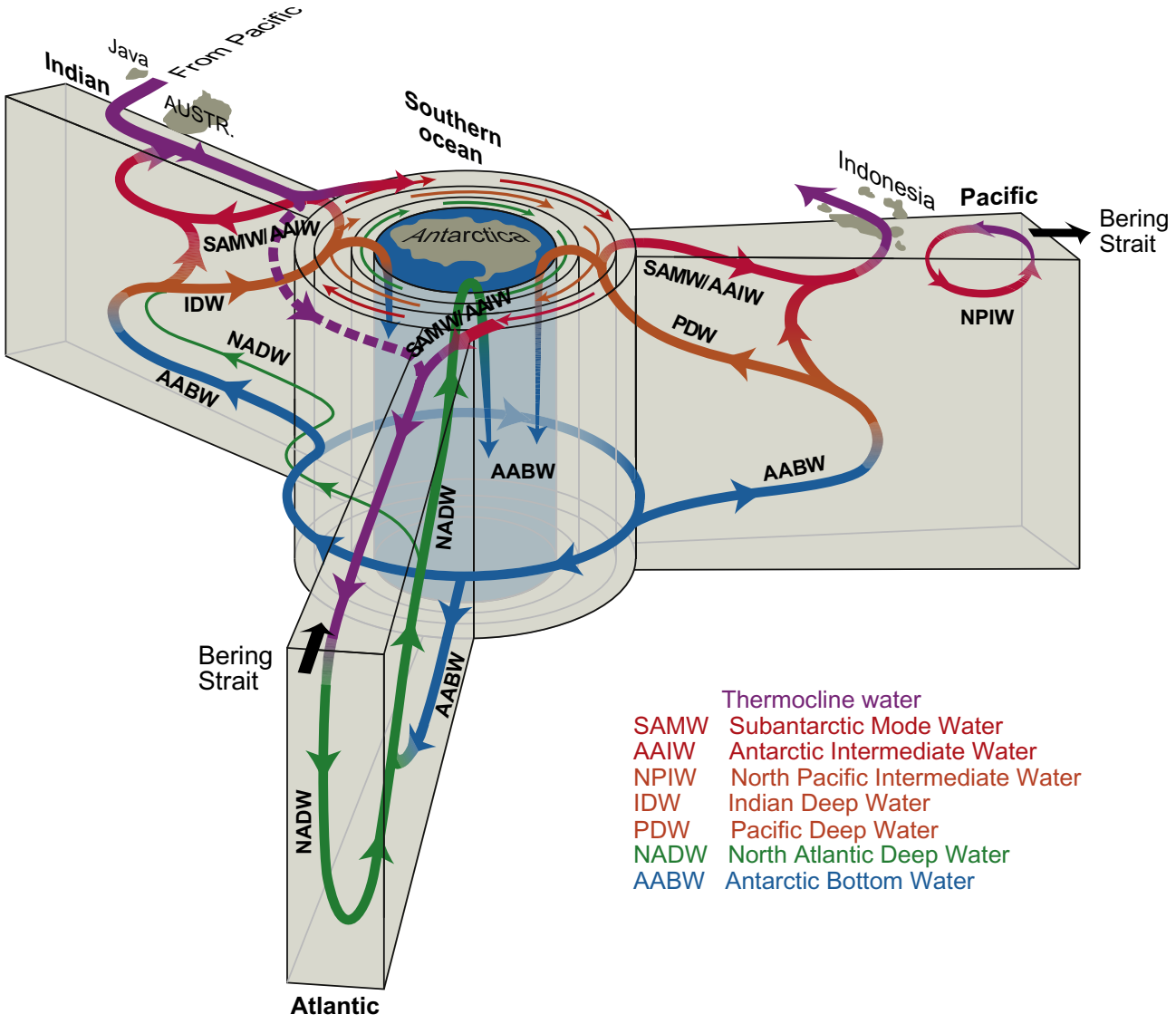

FIGURE 1.8 Highly idealized cartoon-type overview of the deep circulation connecting the three major ocean basins with an indication of the various water masses involved in this flow. *Figure adapted from Talley (2013), based on Schmitz (1996), after Gordon (1991).*

and the locations of the various water masses in the three major ocean basins is given in Figure 1.8. This concept has been useful in highlighting the importance of this circulation in the climate system and has also been inspiring for the understanding of abrupt climate changes in the past (Broecker and Denton, 1989; Stocker and Wright, 1991; Stocker, 2000; Clark et al., 2002). However, modern oceanography with the growing dataset of autonomous measurement devices deployed in the ocean (Chapter 3) (Roemmich and Gilson, 2009), dedicated arrays (Johns et al., 2011), a rich variety of satellite products (Chapter 4) (Hurlburt et al., 2009), and high-resolution ocean modeling (Chapters 20 and 22) (Maltrud and McClean, 2005) paints a complex picture of a turbulent ocean which, only in the multidecadal time, may bear some similarities with the cartoon-type view presented in Figure 1.8.

Turning briefly back to the question of the closure of the meridional heat transport in the ocean, which suggested the existence of a deep ocean circulation, we estimate the contribution of the overturning circulation in the Atlantic to the total meridional heat flux. Of the 36 Sv of deep water formed globally about 15 Sv are estimated to come from the North Atlantic (Ganachaud and Wunsch, 2000). As above, we can now calculate the heat that is carried in the North Atlantic by a northward flow of 15 Sv of warm surface waters at about 20 °C and an equal amount of cold NADW flowing southward at about 3 °C. These assumptions yield $F_H \approx 1.0 \times 10^{15}$W which is about four times the heat flux transported by the near-surface horizontal gyre

circulation. The calculated estimates of the gyre and the meridional overturning circulation together are in good agreement with the observed value in the North Atlantic (see Figure 1.5a). In the North Pacific, on the other hand, overturning is only shallow and much less heat is carried northward (Talley, 2003).

5. LARGE-SCALE MODES OF VARIABILITY INVOLVING THE OCEAN

So far, attention has been focused on the global-scale, steady circulation patterns of the world ocean. However, it is well documented that atmosphere–ocean exchange fluxes of heat and freshwater vary also on interannual to multidecadal time scales and thus point to the ocean as an active component of global and regional climate variability. A comprehensive synthesis of nonseasonal, interannual to multidecadal sea-surface temperature variability observed worldwide is given by Deser et al. (2010).

The best studied atmosphere–ocean mode of variability is the ENSO phenomenon (Chapter 24, e.g., Cane, 2005; Deser et al., 2010; Sarachik and Cane, 2010). It is characterized by two anomalous ocean–atmosphere states in the equatorial Pacific Ocean (Figure 1.9). These anomalous states can last for several months to more than a year and recur irregularly on a typical time scale of 2–7 years: (i) El Niño with anomalous warm sea-surface temperatures in the eastern tropical Pacific, regionally reduced atmospheric pressure causing the trade winds to weaken there, and an equatorial rain band that extends from Indonesia into the central Pacific; (ii) La Niña with the opposite changes resulting in colder sea-surface water and higher atmospheric pressure in the eastern tropical Pacific, due to a shoaled thermocline and hence stronger coastal upwelling, in response to stronger trade winds. Paleoclimate reconstructions demonstrate the presence of this variability at least during the last millennium (Cobb et al., 2003), but possibly during the past 20,000 years (Rein et al., 2005). During the last 7000 years, no systematic trends in this variability could be detected (Cobb et al., 2013). This mode therefore appears to be a very stable feature of interannual variability in the climate system.

The important role the ocean plays in this mode of variability is evident in Figure 1.9. The vertical movements of the thermocline in the eastern part of the equatorial Pacific influence sea-surface temperatures and thus modify the strength of the trade winds. Atmosphere and ocean are coupled to produce a positive feedback, the *Bjerknes feedback* (Bjerknes, 1969), which is at the heart of the ENSO phenomenon (Cane, 2005). Stronger trades in the eastern equatorial Pacific cause the thermocline to rise through Ekman suction, which in turn produces colder sea-surface temperatures that tend to promote subsidence in the overlying atmosphere. An increase in the high pressure over the eastern equatorial Pacific follows, which further strengthens the trades and closes this positive feedback loop. But the Bjerknes feedback alone cannot explain the recurrence of ENSO. The oscillation involves wave propagation in the ocean: Kelvin waves travel toward the eastern boundary of the Pacific basin where, in turn, the perturbations generate Rossby waves, which then propagate westwards and into the basin off the equator. Together they modify the position and structure of the thermocline in such a way that the system is "recharged" after some years (Wang, 2001). Although basic aspects of this coupled atmosphere–ocean phenomenon are simulated by many comprehensive climate models, ENSO events in only a few models have occurrence frequencies similar to those observed (Guilyardi et al., 2009).

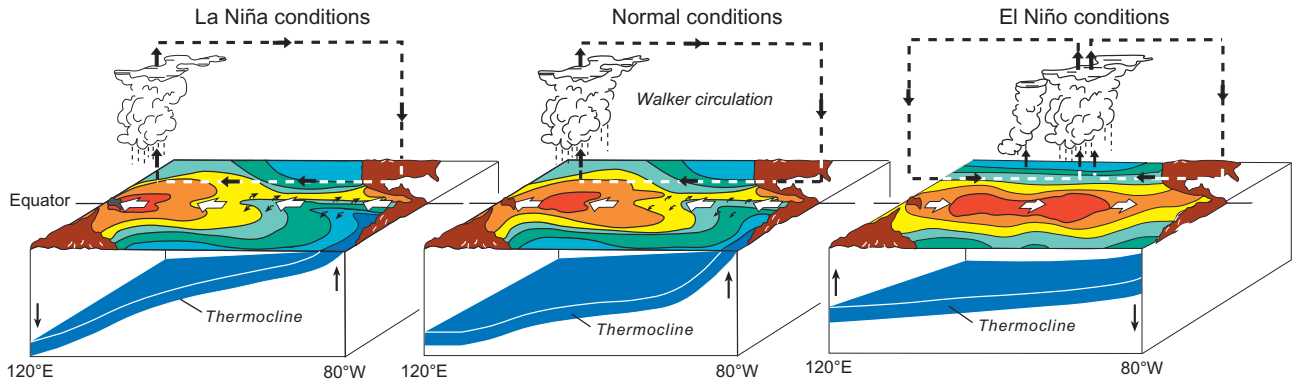

FIGURE 1.9 Schematic illustration of the normal conditions in the equatorial Pacific and two different phases of the El Niño–Southern Oscillation phenomenon. Normal conditions show an east–west gradient in sea-surface temperature (SST) in the equatorial Pacific with a western Pacific warm pool where convective rainfall occurs. The SST gradient is maintained by well-established trade winds with subsidence over the cold pool in the east and convection in the west as part of the Walker Circulation. The trade winds maintain the slope of the thermocline in the equatorial Pacific which, in turn, sets up the SST gradients. During an El Niño event, the trade winds slacken, SSTs warm across the equatorial Pacific, and the convective rain band extends and moves east. As the trade winds weaken, the thermocline relaxes downward. The opposite changes are observed during a La Niña event. El Niño conditions typically prevail from December through February. *Figures adapted from the PMEL TAO Project.*

While ENSO is generated and maintained by processes in the equatorial and tropical Pacific, teleconnections caused by ENSO have been documented around the world (Ropelewski and Halpert, 1987; Halpert and Ropelewski, 1992). The most notable phenomena during El Niño events are dry conditions over Indonesia, Australia, and southeastern Africa, wet conditions in Peru, Ecuador, and the Gulf of Mexico, and warm anomalies in northwestern North America up to Alaska. Effects of ENSO can also be identified to reach Europe (Brönnimann, 2007). Such teleconnections may be difficult to distinguish from the Pacific Decadal Oscillation (PDO; Deser et al., 2004), or other interannual to multidecadal variability that generate teleconnections (Liu and Alexander, 2007).

Also in the tropical Indian Ocean, a basin-wide mode of variability involving strong ocean–atmosphere interaction has been found in observations (Saji et al., 1999; Webster et al., 1999). It is now referred to as the Indian Ocean Dipole (IOD) and is a dominant feature of Indian Ocean variability (Schott et al., 2009). In its positive phase, sea-surface temperatures off the coast of Sumatra are colder, while they are anomalously warm in the western Indian Ocean. The colder temperatures west of Sumatra may be triggered by anomalous seasonal upwelling (Xie et al., 2002) which leads to atmospheric subsidence and stronger easterly winds along the equator. They reinforce the upwelling. This also constitutes the western branch of the Walker circulation in the atmosphere, which leads to convection over the warmer western Indian basin. The rising air enhances rainfall in the western part of the Indian Ocean and in eastern equatorial Africa. This is, again, the Bjerknes feedback, which sets up the prominent dipole pattern in sea-surface temperature in the tropical Indian Ocean. Overall, the physical processes in the tropical atmosphere and ocean that are at work for IOD are similar to those for ENSO.

IOD events are seasonally phase locked and tend to be significantly shorter than ENSO events. While many of the processes that operate during an IOD are also fundamental to ENSO, there are distinct differences that are primarily caused by the strong, thermally driven land–ocean interactions in the Indian Ocean (Li et al., 2003). The warming over the western Indian Ocean induces enhanced evaporation and cloud cover which dampens the warming. It also strengthens the Indian summer monsoon circulation with consequent stronger winds and enhanced mixing in the ocean surface (Webster et al., 1999). All this contributes to a more rapid demise of the IOD, which typically only lasts for a few months, with the strongest phase in October. In the past 40 years, IOD and ENSO did not occur synchronously (Saji et al., 1999) which suggests that they can operate independently. However, through the atmospheric Walker circulation in the tropical Indo-Pacific region, and further teleconnections in the atmosphere, it is not surprising that there are also phases of interaction between IOD and ENSO (Luo et al., 2010), for example, during the prominent IOD event in 1997, and the strong ENSO that unfolded in 1997/1998. IOD events thus may even trigger ENSO (Izumo et al., 2010).

IOD events were inferred from coral records extending over the past 6500 years (Abram et al., 2007). IOD events and associated changes therefore appear to be a persistent feature of tropical variability in the Indian Ocean, but the proxy records indicate that the duration of IOD events was longer during the middle Holocene resulting from a stronger Indian monsoon then. East African rainfall and drought changes found in paleoclimate records covering the past millennium also point to active IOD modes (Verschuuren et al., 2000; Mölg et al., 2006).

The PDO (Chapter 25) manifests itself as warm and cold anomalies of monthly North Pacific sea-surface temperature from November to March (Mantua and Hare, 2002; Deser et al., 2010). PDO variability is not periodic but shows power in two time windows of 15–25 years and 50–70 years. Paleoclimate reconstructions suggest that the PDO is a robust feature during the past 1000 years but the typical time scales of variations may not have been stable (MacDonald and Case, 2005; Shen et al., 2006). The mechanism of this atmosphere–ocean mode is not fully understood. While forcing due to ENSO teleconnections and reemergence of sea-surface temperature anomalies may play roles, stochastic forcing and modulation by the ocean appear to be dominant (Liu, 2012).

Multidecadal variations (Chapter 25) on time scales of 40–60 years and 50–90 years have been found both in coupled model simulations (Delworth et al., 1993) and in the analysis of observed surface temperature records (Schlesinger and Ramankutty, 1994; Sutton and Hodson, 2003). Both studies pointed to the North Atlantic as the center of action. This phenomenon is now referred to as Atlantic multidecadal oscillation (AMO) and is described by basin-wide, coherent sea-surface temperature anomalies in the Atlantic north of the equator (Deser et al., 2010). These anomalies are closely linked to the meridional overturning circulation in the Atlantic, and both temperature and salinity anomalies may be involved (Ou, 2012). When the overturning is stronger, warm anomalies are produced, and also saltier waters are advected northward along the western boundary. This provides a positive feedback for the overturning. Finally, a warm pool will develop and a geostrophic response results in an anticyclonic circulation which brings colder waters from the north to the mid-basin of the Atlantic Ocean, closing the cycle. This suggests that the typical time scale of the AMO may be determined by the volume of water that participates in this variability, which may explain the irregularity found in model simulations and paleoclimatic reconstructions (Gray et al., 2004). AMO might also influence the September sea ice extent in the Arctic (Day et al., 2012). Recent simulations over the twentieth century using coupled climate models show variability

on this time scale but underestimate the amplitude and associated large-scale regional patterns of variation (Kavvada et al., 2013).

6. THE OCEAN'S ROLE IN PAST CLIMATE CHANGE

In order to understand and quantify the sensitivity of the ocean circulation to perturbations and its response to future changes in the major drivers, a combination of approaches, including multiproxy paleoclimate reconstructions and modeling, must be taken. Climate simulations using comprehensive coupled atmosphere–ocean models provide us with estimates of changes in ocean status and circulation for past climates (Braconnot et al., 2012). Understanding the ocean in the context of past climate change (Chapter 2) offers a complementary and increasingly quantitative insight into how the ocean has responded to rather large changes in the forcing fluxes and knowledge that is relevant to assess future changes in ocean status and circulation (see Section 7).

A few numbers demonstrate that the ocean played an important role in past climate change. The world ocean was the principal carbon storage during the course of the ice ages when atmospheric CO_2 concentrations changed between about 180 ppm during an ice age and about 280 ppm during interglacials (Lüthi et al., 2008). Global mean surface air temperatures during the Last Glacial Maximum (LGM, 26,000 to 20,000 years before the present) were about 4–7 °C colder than today (Jansen et al., 2007; Masson-Delmotte et al., 2013). Global mean cooling at the ocean surface during the LGM has been recently estimated at about 2 °C (MARGO Project Members, 2009), but for large areas with likely much larger cooling no reconstructions are available (Figure 1.10). Deep ocean temperatures were near the freezing point (Adkins et al., 2002). During the LGM, sea level was about 130 m lower than today (Clark et al., 2009; Church et al., 2013), whereas about 125,000 years ago, in the previous interglacial, it was 5.5–9 m higher than today (Dutton and Lambeck, 2012). These sea-level variations impact directly on the mean salinity of the world ocean with today's mean salinity being about 1.1 units lower than at the LGM.

Wind patterns during the last glacial period were significantly different from today due to the presence of the northern hemisphere ice sheets, more extended sea ice cover, and changed meridional temperature gradients. Although their

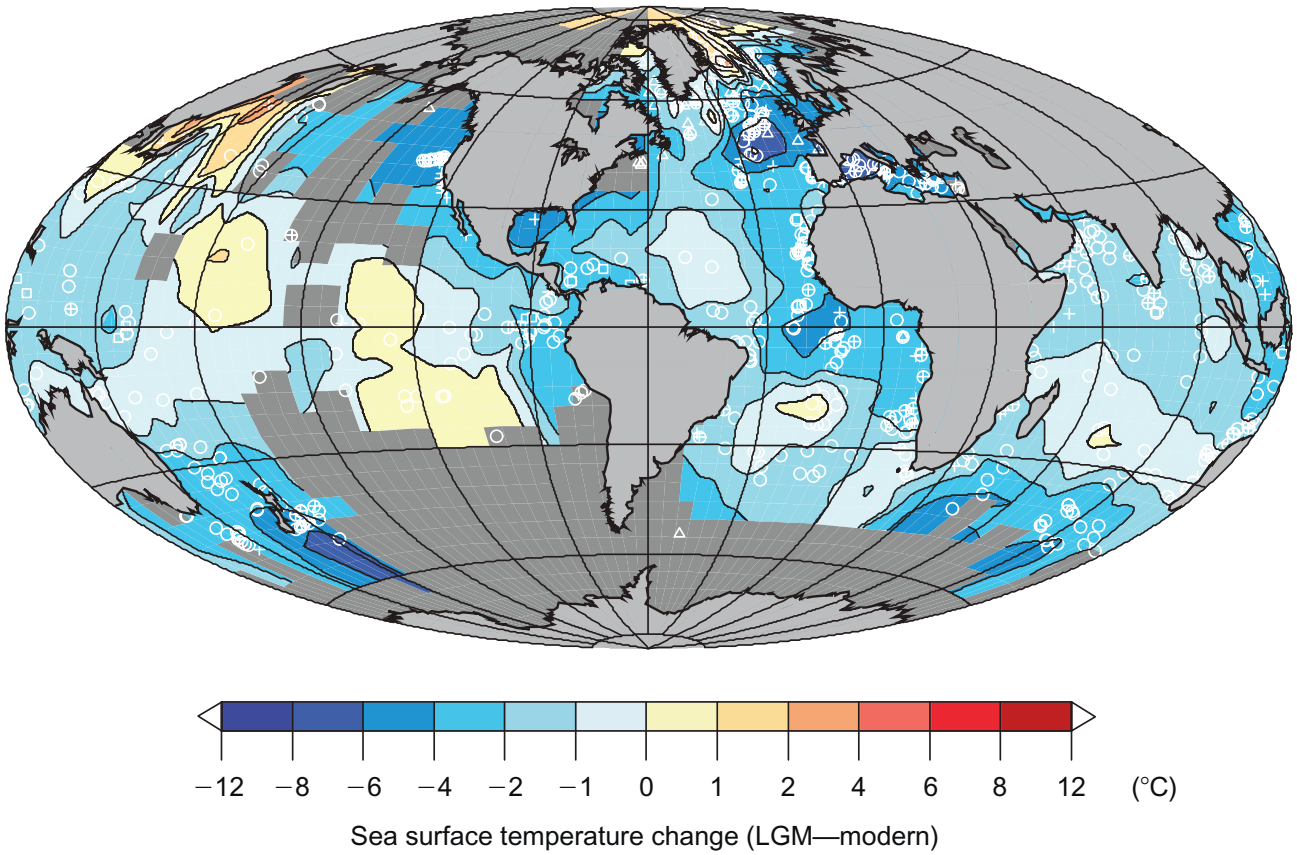

FIGURE 1.10 Reconstructions of annual mean sea-surface temperatures anomalies at the Last Glacial Maximum relative to today, based on a multiproxy approach using several paleothermometers. Uncertainties are large, and data coverage in large dynamically essential areas of the ocean, for example, the Southern Ocean, is poor or missing. *Figure from MARGO Project Members (2009).*

strength has likely changed, zonal wind belts still forced the surface gyre circulation, making it a robust feature of the ocean circulation throughout the ice age cycles.

Unfortunately, reconstructions of sea-surface salinity distributions in the past are still scarce and highly uncertain, but there is indication of a change in the east–west surface salinity gradient in the North Atlantic (Schäfer-Neth and Paul, 2003). During most of the last ice age, the Bering Strait was closed because sea level was below the depth of this shallow passage. With the Bering Strait closed, the Arctic salt balance and the Arctic–North Atlantic water exchange were very different from today. Together with modified air–sea fluxes and sea ice cover, it is therefore not unreasonable to expect major changes in the strength and structure of the deep circulation of the ocean in the past. Model simulations suggest that this closure also modified the sensitivity of the meridional overturning circulation to freshwater perturbations (Hu et al., 2012).

A major effort in paleoceanography therefore concerns the reconstruction of the ocean circulation in the past, in particular the ocean circulation during the LGM and its transient evolution to the circulation observed today. The rationale is that by documenting and understanding in detail how the ocean circulation operated during the last ice age, and during the transition to the Holocene leading up to the present, a wide variety of ocean states could be "sampled", which would allow us to capture the essential dynamic range of the ocean to perturbations and changes in the different forcing factors.

A palette of different physical and geochemical indicators measured on marine sediments has been developed to quantify changes in water mass characteristics of the ocean in the past (Lynch-Stieglitz, 2003). The stable isotope ratios of oxygen ($^{18}O/^{16}O$) and carbon ($^{13}C/^{12}C$), measured on the calcareous shells of different organisms, are widely used paleoceanographic quantities from which changes in temperature, water mass distribution, and sea level are inferred. Temperature information as in Figure 1.10 is also derived from Mg/Ca ratios and concentrations of alkenones; metal tracers such as Pa, Th, and Nd, and their isotopes, provide further constraints for changes in water masses (Rempfer et al., 2011).

With the growing number of paleoceanographic indicators and related datasets, it should therefore eventually be possible to assimilate the information into an ocean circulation model and reconstruct the past circulations employing the same approach of inverse modeling as for modern data. Such a study indicates that the deep circulation in the Atlantic Ocean of today is incompatible with the tracer distributions reconstructed for the last glacial (Marchal and Curry, 2008). Based on nutrient tracers, one can infer that the large-scale water mass distribution in the glacial Atlantic was dominated by a shallower water mass, Glacial North Atlantic Intermediate Water, lying over a more widespread AABW (Lynch-Stieglitz et al., 2007), and possibly reduced mixing between northern and southern water masses (Lund et al., 2011). However, various model simulations still give conflicting results for the Atlantic overturning strength during the LGM (Otto-Bliesner et al., 2007), and recent numerical model results suggest some threshold behavior of the overturning circulation with respect to the surface buoyancy flux and wind stress forcings (Oka et al., 2012).

An intriguing feature of past climate change, for which the ocean is thought to be a major player, is the sequence of 26 abrupt warmings as recorded in the Greenland ice core record (Stocker, 2000; North Greenland Ice Core Project members, 2004). The most recent and last in the series of these warmings occurred 11,650 years ago and marked the beginning of the current warm period, the Holocene. These events are commonly referred to as Dansgaard–Oeschger events in honor of the Danish and Swiss scientists *Willy Dansgaard* (1922–2011) and *Hans Oeschger* (1927–1998) who identified and interpreted them in the first deep ice cores from Greenland (Dansgaard et al., 1984) and noted their widespread climatic significance (Oeschger et al., 1984). The warmings in Greenland occur extremely rapidly, sometimes within a few years (Steffensen et al., 2008), and have amplitudes of 8° to 15 °C (Huber et al., 2006). Many independent indications from reconstructions of temperature and precipitation changes on land, sea-surface temperature changes, changes in water mass indicators in the ocean, and global-scale spatial correlations strengthen the view that the ocean, in particular the Atlantic overturning circulation, has played a fundamental role in these climate variations (Broecker and Denton, 1989; Stocker, 2000; Clark et al., 2002; Voelker and Workshop-Participants, 2002; Alley et al., 2003; Clement and Peterson, 2008; Fleitmann et al., 2009). This is because more than 75% of the heat transport in the North Atlantic Ocean depends on the overturning circulation (see Section 4), and variations of its strength are an efficient regulator of regional climate in this region. If this "heat pump" is switched off, a substantial impact on sea-surface temperatures and the atmosphere is expected.

A large body of climate model simulations, ranging from simplified conceptual models to comprehensive coupled climate models, demonstrates that the AMOC sensitively responds to changes in the surface buoyancy balance and the distribution of wind stress. Some studies argued that the overturning circulation has multiple equilibria (Stommel, 1961; Manabe and Stouffer, 1988; Stocker and Wright, 1991). Such a property would create hysteresis, with the surface freshwater balance in the North Atlantic being an important determinant which, depending on the climate state, could create the possibility of abrupt climate change in response to perturbations in the freshwater balance (Stocker and Marchal, 2000; Hu et al., 2012). The most

effective perturbation of this kind during the last ice age was recurring massive iceberg discharges from the northern hemisphere ice sheets and Antarctica. Such an iceberg flow into the ocean would result in large freshwater lenses disrupting the deep water formation and hence reduce the oceanic meridional heat flux in the North Atlantic.

Direct identification of past changes in the AMOC remains a challenge as there are only indirect paleoceanographic indicators registering such changes. Metal tracer concentrations (Pa, Th, and Nd) and their isotopic ratios inform about water mass distributions and are, unlike the carbon isotopic ratios, less influenced by couplings with the carbon cycle. They therefore offer a way to quantitatively determine changes of the meridional overturning circulation in the past (Piotrowski et al., 2004). Model simulations suggest that such tracers may be able to quantify such changes in response to freshwater discharges from the north or the south, and discriminate between them (Rempfer et al., 2012). Time-resolved reconstruction of sea-surface temperature distributions also holds promises to quantify AMOC changes (Ritz et al., 2013).

Currently, the most convincing evidence for a large involvement of the meridional overturning circulation in the sequence of Dansgaard–Oeschger events during the last ice age comes from the remarkable interhemispheric coupling of these abrupt warmings. Today, the meridional heat flux in the Atlantic Ocean at 30°S is directed northward (Figure 1.5), and therefore this ocean imports heat from the Southern Ocean when the overturning circulation is operational. The paleoclimatic significance of this cooling effect of the Southern Ocean was recognized by Crowley (1992). Rapid changes of the Atlantic overturning circulation are therefore expected to produce climate signals of opposite sign in the South Atlantic Ocean to those in the North Atlantic Ocean, and by ocean–atmosphere coupling, in the overlying atmosphere. This led to the formulation of the "bipolar seesaw" hypothesis (Broecker, 1998; Stocker, 1998).

Ice cores from Greenland and Antarctica offer the unique possibility of producing highly time-resolved climate records that can be placed on one synchronized time scale by employing the rapid changes in the methane concentrations measured on these cores as a reliable global time marker. This approach revealed an asynchronous behavior between Greenland and Antarctica for the Antarctic warmings during the last ice age (Blunier et al., 1998; Capron et al., 2010). While abrupt warmings in Greenland are followed by millennial-scale coolings, temperature variations inferred from Antarctica isotope records were more gradual during the last ice age. A consistent pattern is that the Antarctic warming trends change into cooling trends at the time of the abrupt warming in the Greenland ice cores, that is, synchronous with the Dansgaard–Oeschger events. The fundamentally different temporal character of these events—abrupt in the north and gradual in the south—could be resolved by postulating a thermal damping influence of the large Southern Ocean heat reservoir (Stocker and Johnsen, 2003). Two testable predictions followed from this model of the "thermal bipolar seesaw": (i) all Dansgaard–Oeschger events should produce a warming in Antarctica and (ii) the duration of the cooling in Greenland is proportional to the amplitude of the warming in Antarctica.

The ice core from Dronning Maud Land in Antarctica produced a temperature record of significantly higher time resolution than previous Antarctic records. Moreover, the ice core is located in the South Atlantic sector of Antarctica and hence in an area which is expected to react particularly sensitively to the bipolar seesaw (EPICA Community Members, 2006). When synchronized onto the time scale of the Greenland ice core (North Greenland Ice Core Project members, 2004), each Dansgaard–Oeschger event could be associated with a corresponding Antarctic Isotope Maximum event (Figure 1.11). Further, the proportionality postulated by the thermal bipolar seesaw was also confirmed (EPICA Community Members, 2006; Capron et al., 2010). This remarkably coherent interhemispheric coupling persisted through the transition from the last ice age into the Holocene (Barker et al., 2009). Using the seesaw concept in an inverse approach, it can be suggested that Dansgaard–Oeschger events were a common feature of at least the past 800,000 years (Siddall et al., 2006; Barker et al., 2011). In summary, these results demonstrate the important global-scale role of changes in the ocean circulation for abrupt climate change and variations on the centennial-to-millennial time scale in the past.

Finally, the ocean is also the key climate system component to enable glacial–interglacial changes in atmospheric CO_2 (Fischer et al., 2010). Ice core records indicate CO_2 variations of about 100 ppm during the past eight ice age cycles (Lüthi et al., 2008). During the LGM, atmosphere and land together held about 400–800 Gt carbon less than today (Sigman and Boyle, 2000). This extra carbon must have been stored in the ocean and in sediments, and this required substantial physical, chemical, and biological changes in the ocean to permit the observed reduction in atmospheric CO_2. During the LGM, the sea-surface temperature was about 2 °C colder (Figure 1.10), which increases the solubility of CO_2 and reduces atmospheric CO_2 by about 20 ppm. As pointed out above, the uncertainty in this estimate is very large. The increase in salinity partially offsets this reduction by about 10 ppm. Other physical changes involve shifts in water mass distributions, larger sea ice cover, and increased stratification in the Southern Ocean, but these physical effects together are able to account for only about a third of the required reductions in atmospheric CO_2. Ocean chemistry was therefore also involved in the glacial–interglacial CO_2 changes. An increase in the ocean's alkalinity would

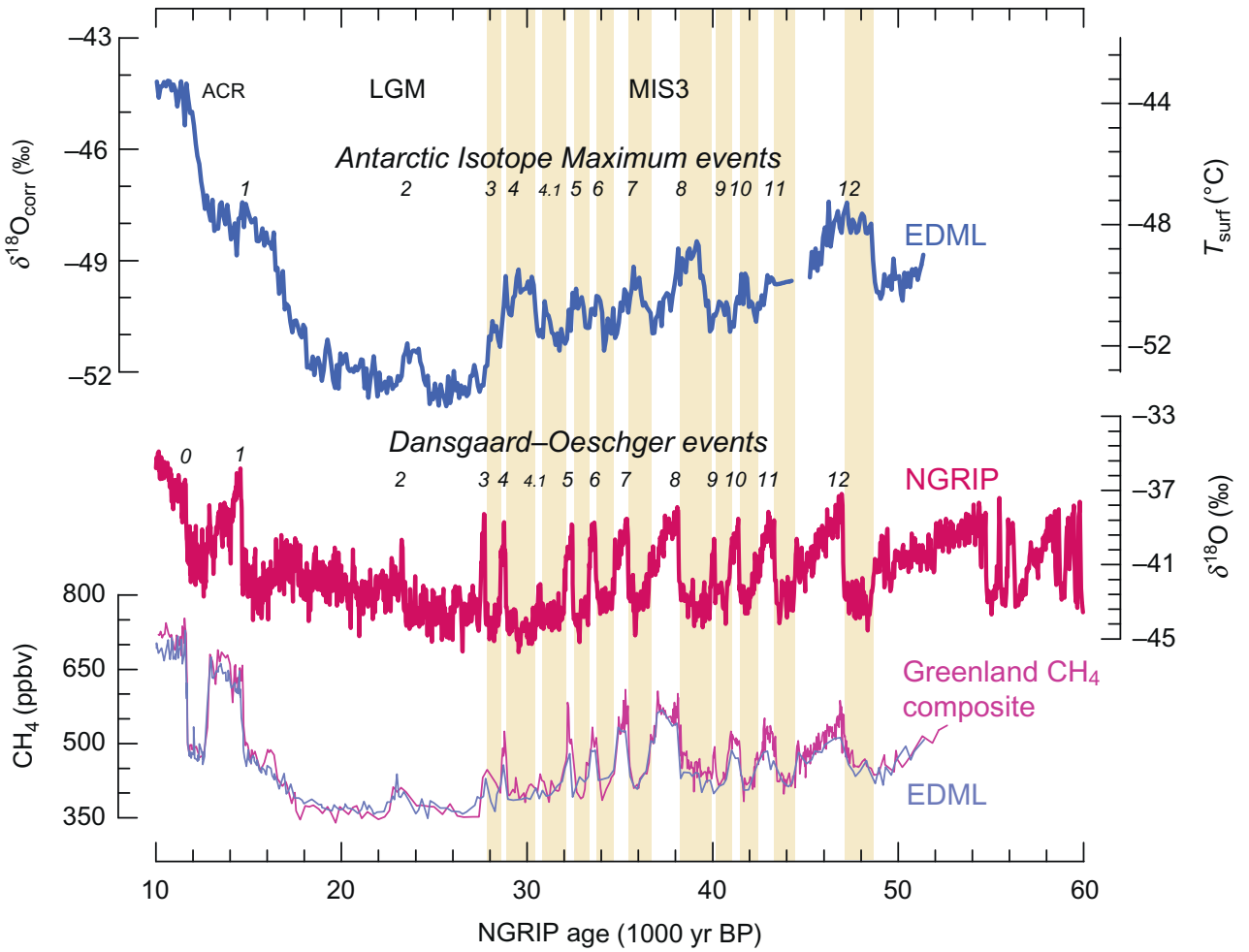

FIGURE 1.11 Sequence of abrupt climate changes during the Marine Isotope Stage 3 (MIS3) as recorded in ice cores from Antarctica (EDML, EPICA Dronning Maud Land) and Greenland (NGRIP, North Greenland Ice Core Project). The combination of these key paleoclimatic records provides convincing evidence for the role of the Atlantic meridional overturning circulation in determining the interhemispheric coupling during the last ice age. Gradual warmings and coolings in Antarctica (Antarctic Isotope Maximum events) occur synchronously with abrupt warmings in Greenland (Dansgaard–Oeschger events). This coherent interhemispheric coupling persists through much of the last ice age (Capron et al., 2010). During the Last Glacial Maximum (LGM), these events are absent or subdued; during the transition to the Holocene, the sequence reappears with the abrupt warming in Greenland at 14,500 years before the present (Dansgaard–Oeschger event 1), the Antarctic Cold Reversal (ACR), and Dansgaard–Oeschger event 0 being the last such abrupt event (Stenni et al., 2011). *Figure modified from EPICA Community Members (2006).*

also reduce atmospheric CO_2. This can be caused by changes in the calcium carbonate cycle on land (increase in weathering), in the ocean (reduced growth of coral reefs, a decrease in the production ratio of carbonate/organic carbon), or in the sediment (reduced carbonate burial).

Changes in the biological processes are also invoked to explain the glacial–interglacial CO_2 changes. More dust in the atmosphere during the ice age may have supplied more iron, a nutrient which could stimulate marine productivity and burial of organic matter.

None of these mechanisms, individually, is able to explain quantitatively the carbon cycle changes during a glacial–interglacial cycle (Kohfeld and Ridgwell, 2009). Therefore, a temporally coordinated succession of processes involving ocean physics, chemistry, and biology must have been at play to produce the observed tight relationship between reconstructed air temperatures and atmospheric CO_2 concentrations (Siegenthaler et al., 2005). Coupled climate–carbon cycle models begin to capture the complexity of these transient changes but are not yet able to quantitatively simulate ice age variations in a way that is fully consistent with the paleoclimatic and paleoceanographic evidence (Menviel et al., 2012).

7. THE OCEAN IN THE ANTHROPOCENE

The anthropocene is a new era during which human activities profoundly change the Earth System, by burning of fossil fuels, changing land use, and by deforestation. These impacts on all components of the climate system are now

well documented (IPCC, 2007, 2013) and can, in many cases, be attributed to the direct and indirect effects of the increase of greenhouse gases in the atmosphere on global and regional scales (Stott et al., 2010; Bindoff et al., 2013). Although changes in the ocean are challenging to detect due to the large volume and the relative scarcity of observations, the ocean is an excellent integrator of changes owing to the long time scales involved in ocean processes. As already shown in Table 1.1, fundamental properties have been observed to change (Chapters 27, 28, and 30). Melting glaciers and ice sheets add mass to the ocean, thermal energy penetrates the ocean due to the widespread and long-term warming of the lower atmosphere observed in the twentieth and the beginning of the twenty-first century, a stronger atmospheric branch of the hydrological cycle causes a redistribution of salinity in the global ocean (Bindoff et al., 2007; Rhein et al., 2013), and the continuous rise of CO_2 in the atmosphere causes an ocean uptake of carbon (Rhein et al., 2013). All these changes have consequences for ocean circulation, distribution of water mass properties, and the chemical status of the ocean.

This is evident from the global zonal averages of the most recent data survey (Durack and Wijffels, 2010), and shown in Figure 1.12. A total of about 24×10^{22} J have entered the world ocean since 1955 (Levitus et al., 2012). The warming can be detected to be essentially global in the top 700 m of the ocean, and recent studies indicate that this is induced by human activity (Gleckler et al., 2012). In the Atlantic Ocean, the warming reaches deeper to about 2000 m because NADW transports the warmer waters efficiently to that depth (Figure 1.7). Since the 1990s, a small downward heat flux crossing 4000 m depth could be observed, which amounts to about 10^{12} W (Purkey and Johnson, 2010), thus less than 1% of the anthropogenic heat flux at the surface (Table 1.1). The time span of these observations is still too short to determine whether this is an anthropogenic signal or natural variability. The global extent of the signal and simple physical arguments, however, rather suggest this to be the early sign of whole-ocean warming.

The salinity changes in the top 500 m of the world ocean are significant and show a consistent pattern of freshening in the tropics and the high latitudes of both hemispheres, while the extra-tropics show increasing salinity (Durack and Wijffels, 2010). This is the signal that would be expected from an "accelerating" hydrological cycle: more water is evaporated in the dry zones of the subtropical gyres and more precipitation would occur in the high latitudes implying a stronger meridional moisture flux in the atmosphere (Held and Soden, 2006; Durack et al., 2012). The detection of this important change is facilitated by the integrating property of the ocean for changes in the atmospheric hydrological cycle. This is the response of the water cycle that comprehensive climate models consistently project for the twenty-first century (Meehl et al., 2007; Collins et al., 2013), and it appears that this trend has already started on a global scale.

Both the addition of freshwater from melting glaciers and ice sheets, and the heating from the surface reduce the density of the upper 500 m of the ocean. This strengthens the stratification and thus would likely reduce vertical mixing, which is an essential process in

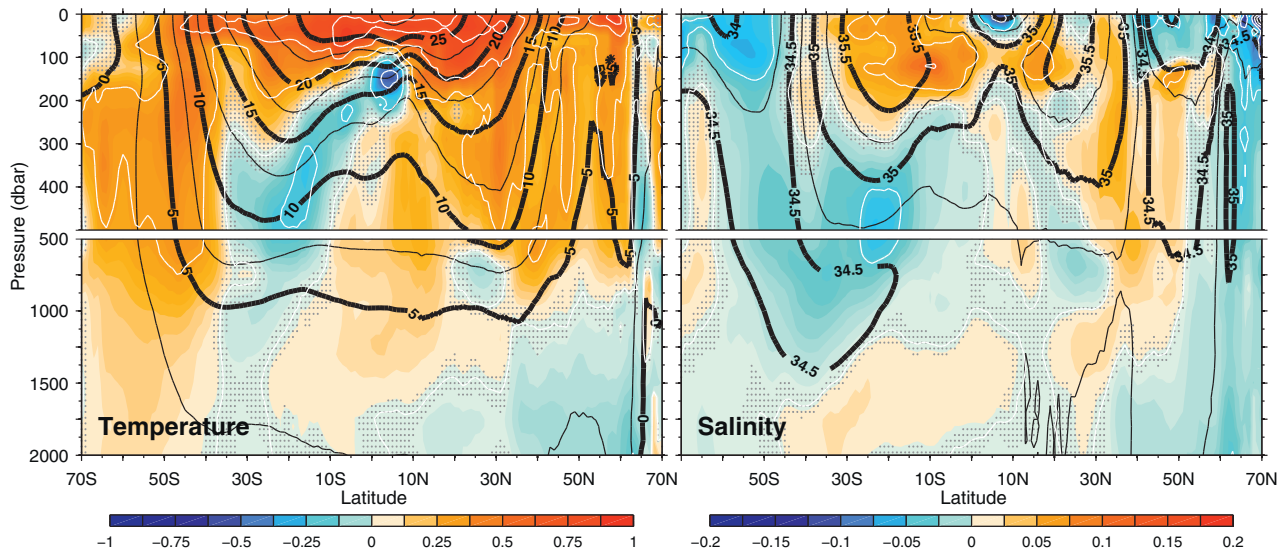

FIGURE 1.12 Global zonal mean 50-year trends of ocean temperature (left) and salinity (right) from 1950 to 2008 down to 2000 m depth. Superimposed black contours mark the zonal mean temperatures and salinities. Areas with trends that are not significant at the 90% confidence level are stippled. *Figure from Durack and Wijffels (2010) and P. Durack, personal communications.*

determining the ocean circulation and formation of water masses (see Section 4). Moreover, warming and freshening are amplified in the high latitudes where deep water is being formed. With both temperature and salinity changes conspiring to lower the densities of surface ocean waters, one would expect that the meridional overturning rates may reduce. Early coupled atmosphere–ocean model simulations (Chapter 23) have indicated the possibility that the ocean circulation may exhibit large-scale changes in deep water formation rates, particularly in the North Atlantic (Manabe and Stouffer, 1994). Most models, in fact, show a decrease of the AMOC in response to increases in greenhouse gas concentrations (Meehl et al., 2007; Collins et al., 2013), although the spread of this reduction is large, ranging from essentially no change to a reduction of 50% by the end of the twenty-first century. But the confidence in the representation of ocean processes determining deep water formation simulated by these models is only moderate.

Guided by insights from the paleoclimatic records, concerns about unpleasant surprises in a warming world were expressed by Broecker (1987a). Particularly, the warming could constitute a perturbation sufficiently strong for the meridional overturning circulation in the Atlantic Ocean to come to a halt. Some even speculated that the warming could trigger an abrupt shutdown of the "heat pump" with severe adverse implications for climate in Europe. However, there is no support from climate models for such extreme scenarios. In fact, as the changes in the AMOC are induced by the warming and the related strengthening of the water cycle, a slow-down of the circulation would only moderate the warming in the North Atlantic region but not lead to a net cooling.

If the AMOC indeed has multiple equilibrium states, as suggested by a number of models (Bryan, 1986; Stocker and Wright, 1991; Stocker and Marchal, 2000; Rahmstorf et al., 2005), the system could show a bifurcation with rising global temperatures. This behavior was suggested in a coupled climate model for the first time by Manabe and Stouffer (1993). In these simulations, the CO_2 concentrations were increased by 1%/yr up to double after 70 years, and quadruple levels after 140 years, and held constant thereafter, which resulted after 500 years of integration in a global mean warming of about 3.5–7 °C, respectively. The Atlantic overturning circulation decreased initially in both simulations, bifurcated then to a near shutdown in the $4\times CO_2$ experiment but recovered in the $2\times CO_2$ case. The slow-down occurred on the time scale of the forcing and was not abrupt. A central question was whether this, at that time comprehensive, model simulation would settle into this new equilibrium state. Later, continuation of these simulations showed that the Atlantic overturning recovered again after more than 1000 years of constant $4\times CO_2$ forcing (Stouffer and Manabe, 2003). This was attributed to a slow deep water warming, which gradually decreased the stability of the North Atlantic Ocean waters and promoted the deep water formation to return.

This early coupled climate model still employed so-called flux-corrections, and hence confidence in this result was limited. However, the most recent simulations with comprehensive models, which couple the different climate system components in a physically consistent way, confirm these early results obtained using simplified models. For high greenhouse concentrations, the occurrence of multiple equilibrium states in the meridional overturning circulation seems to be a robust result that does not depend on the model used (Mikolajewicz et al., 2007; Meehl et al., 2012), nor on its complexity (Stocker and Schmittner, 1997). Multiple equilibria are also found in complex coupled models applied in very different climatic conditions and configurations (Ferreira et al., 2011), suggesting that this is likely a general feature of the ocean in the Earth System.

Figure 1.13 presents an example of a simulation investigating the AMOC's response to an increase in the greenhouse gas concentrations since 1850 (Meehl et al., 2012), including an update (A. Hu, personal communication). The latest emission scenarios for climate model simulations (Moss et al., 2010) are used and extended to the year 2300, to achieve CO_2-stabilization at about 361, 543, 752, and 1962 ppm, which results in global mean warmings of 0.5, 2.2, 3.6, and 8.4 °C, respectively, relative to the mean of 1986–2005 (Figure 1.13a). The simulation using the highest emission scenario are carried further to year 2500 and reach a global mean warming of 9 °C. In these simulations, the response of the Atlantic overturning circulation shows a bifurcation between the warming of 3.6 and 8.4 °C. The evolution of the overturning indicates that the response of the AMOC changes fundamentally between the two highest scenarios. Whereas for the three lower scenarios, the circulation reduces but then recovers to almost the original value, for a higher forcing, the circulation spins down and almost vanishes by year 2200. That this seems to be a new stable state for at least several centuries is indicated by the continuation of this simulation up to year 2500. Therefore, a bifurcation point for the AMOC appears to exist in this model in which at a specific warming, and associated changes of the water cycle, a transition to a new equilibrium is triggered. The bifurcation already occurs between years 2020 and 2040 in these simulations, when the temperature differences between the scenarios are still rather small. The fact that a bifurcation is simulated demonstrates that there could be intrinsic irreversibility in the climate system. The Atlantic overturning circulation is not the only component in the climate system for which models have found such "points of no return."

The occurrence of bifurcation in the AMOC also depends on the history of the warming (Stocker and Schmittner, 1997). Thresholds are thus not absolute but

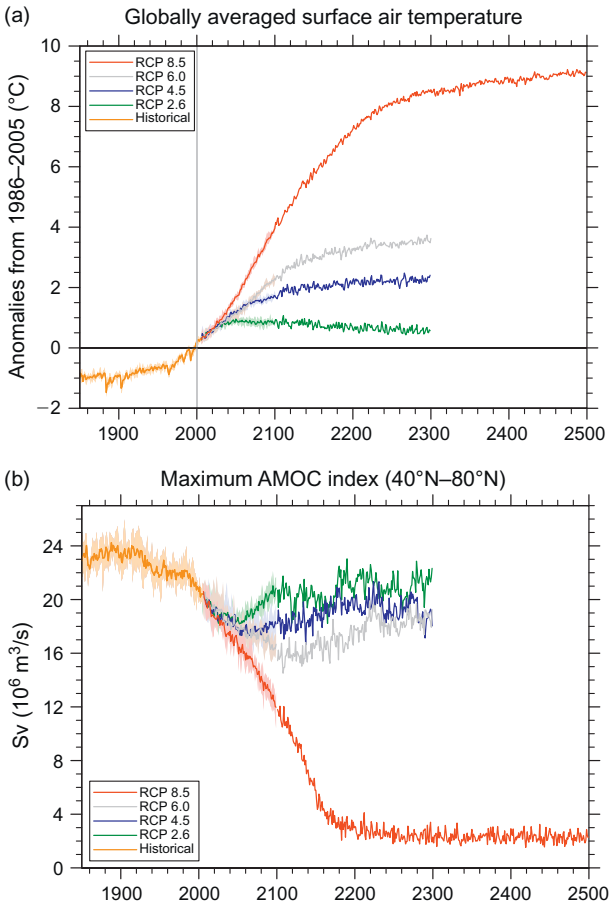

FIGURE 1.13 Projections of global mean temperature change (referenced to 1986–2005) (a) and Atlantic meridional overturning circulation (b) using a comprehensive coupled climate model (CCSM4) forced with concentrations from four greenhouse gas emission scenarios. *Figure based on Meehl et al. (2012) and updated by A. Hu (personal communication).*

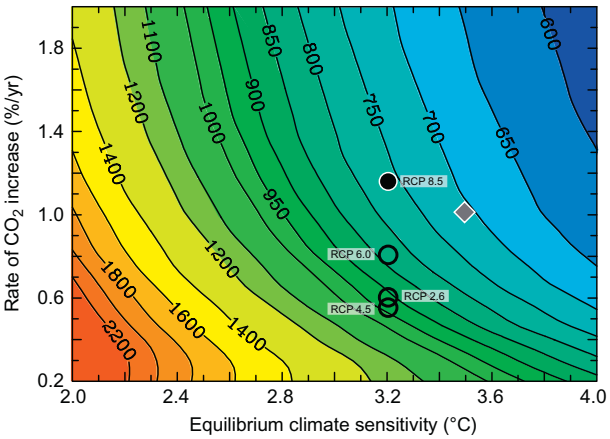

FIGURE 1.14 Contours of threshold CO_2 concentrations beyond which a bifurcation of the Atlantic meridional overturning circulation (AMOC) is simulated using a coupled model of reduced complexity that shows bistability of the AMOC. The threshold concentration depends on climate sensitivity and the rate of the CO_2 increase, and hence the warming. Circles indicate simulations presented in Figure 1.13 forced by the four emission scenarios RCP 2.6 to RCP 8.5. The AMOC recovers when the CO_2 concentrations remain below the threshold (open circles), but the AMOC shuts down if the CO_2 concentrations exceed the threshold (filled circle). The gray diamond indicates the early simulations by Manabe and Stouffer (1993) which showed an AMOC shutdown for more than 1000 years and a subsequent slow recovery over several centuries. *Figure modified from Stocker and Schmittner (1997).*

may be avoided if different emission pathways are chosen. This is best illustrated in simple scenarios in which the atmospheric CO_2 concentration is increased at a given fraction per year until a value is reached and the concentration is held fixed thereafter (Manabe and Stouffer, 1993; Stocker and Schmittner, 1997). Figure 1.14 shows the critical CO_2 concentrations beyond which the AMOC assumes the new equilibrium state of shutdown. Results are obtained from many simulations using a coupled ocean–atmosphere model of reduced complexity that has two stable equilibrium states of the AMOC (Stocker et al., 1992; Stocker and Schmittner, 1997). It is evident that increased climate sensitivity and more rapid emissions both lower the CO_2 threshold. Therefore, a shutdown can be avoided by choosing a slower path to the same eventual CO_2 level. The reason for this rate-dependent stability is the fact that a faster increase of greenhouse gas concentrations in the atmosphere and the consequent rapid surface warming of the ocean enhance the stratification of the surface ocean, which reduces deep water formation and the overturning circulation. If the greenhouse gas increase proceeds more slowly, time is given for the heat to penetrate to the deeper layers of the ocean, which avoids the strong vertical density anomalies that would otherwise create an eventual shutdown. This suggests the rate at which the ocean takes up heat must be sufficiently slow to mix away the surface buoyancy increase created by the warming.

Results from some simulations using comprehensive coupled climate models are indicated in Figure 1.14 by symbols. Manabe and Stouffer (1993) report a climate sensitivity of their model of 3.5 °C. In a 1%/year CO_2 increase experiment, the threshold for a shutdown of the AMOC lies between $2\times$ and $4\times$ CO_2 concentration, consistent with the value of about 700 ppm obtained from the simplified model. The model used for the simulations presented in Figure 1.13 has a climate sensitivity of 3.2 °C (Meehl et al., 2012). Taking from every simulation the maximum of the time-varying rate of CO_2 increase as an indicator, the CO_2 thresholds are expected to be above 800 ppm for the three lower emission scenarios which have maximum CO_2 concentrations of about 361, 543, and 752 ppm, respectively. The simulation forced by the highest emission scenario RCP 8.5 reaches a CO_2 concentration of 1962 ppm and a maximum increase rate of 1.15%/year. The threshold predicted by the reduced complexity model is 770 ppm and therefore a bifurcation would be expected, as indeed

simulated by the comprehensive model (Figure 1.13b). This lends strong support to the suggestion that the rate of buoyancy increase in the high-latitude surface ocean, caused by the combination of warming and enhanced meridional transport of freshwater, is therefore one of the determinants for an eventual AMOC shutdown. In order to avoid such a fundamental and long-lasting, if not irreversible, change of the circulation regime in the Atlantic Ocean, not only the level of warming, but also the speed of it, need to be limited. This insight provides a strong physical argument in favor of early and substantial greenhouse gas mitigation efforts.

An important question also concerns the response of the modes of natural variability to climate change. The ENSO phenomenon strongly influences regional climate in the equatorial Pacific region and even has implications on the global scale (see Section 5). Comprehensive climate models are capable of simulating ENSO variability, but many of them have difficulties in being realistic in the amplitude and frequency of occurrence and associated teleconnections. Early model simulations using a coupled climate model with sufficient resolution in the equatorial region showed an increase in the frequency of El Niño situations, and increased cooling during La Niña events, and they attributed this to the strengthening of the equatorial thermocline caused by the warming (Timmermann et al., 1999). However, the analysis of the evolution of ENSO characteristics (frequency and intensity) in both the past and the ongoing coordinated coupled model intercomparison projects does not show conclusive results (Collins et al., 2010; Stevenson, 2012). Some models show a strengthening, some a weakening of ENSO, and even when only those models are considered that exhibit the most realistic present-day ENSO simulations, the results remain, unfortunately, equivocal. Two robust results, however, are that: (i) ENSO continues to be a dominant feature of climate variability in the equatorial Pacific and (ii) none of the models indicates a lock-in into one of the ENSO states in response to the warming. The irregular sequence of warm El Niño and cold La Niña events is very likely to persist, possibly with altered relative frequencies and durations.

One of the longest-term and most certain commitments of the emissions of greenhouse gases is sea-level rise (Cazenave and Llovel, 2010; Church et al., 2013) (Chapter 27). The warming has direct and indirect effects on sea level. First, the well-observed uptake of heat by the world ocean to progressively deeper layers causes the so-called thermosteric contribution to sea-level rise due to the expansion of water as it warms. This contribution is rather well understood and quantified ranging from 0.1 to 0.41 m depending on the scenario by the end of the twenty-first century (Meehl et al., 2007). Second, melting glaciers and ice caps increase sea level but their contributions are projected to be significantly smaller (0.07–0.17 m). Third, the contribution from melting and possibly rapid responses of Greenland and Antarctica are potentially very large. A recent estimate for a dynamical response of the West Antarctic Ice-Sheet estimates an additional 3.3 m of which about 0.8 m may be realized by the end of the twenty-first century in a fast melt scenario (Bamber et al., 2009). However, such estimates and the possible location of thresholds remain highly uncertain (Joughin and Alley, 2011).

An important issue is the long-term commitment by the two contributions of ocean warming and ice sheet melting to global sea-level rise. The thermosteric contribution alone has a very long characteristic time scale, taking many centuries to equilibrate after greenhouse gases equilibrate (Plattner et al., 2008). This is due to the time required for the heat to penetrate to the deepest levels of the ocean. Likewise, the ice sheet melting and adjustment take more than 1000 years to come into equilibrium with the new climate. As before, there is indication that also the large ice sheets may exhibit bifurcation behavior, and thus thresholds for the warming that would preserve the ice sheets may exist (Gregory and Huybrechts, 2006; Robinson et al., 2012). With the recent insight and understanding that warming at the ocean–ice shelf interface is efficiently destabilizing ice streams (Holland et al., 2008), the ocean's crucial role in determining future sea level must be considered, as it influences the two dominant contributions to sea-level rise.

Currently, the ocean takes up carbon at the rate of about 2.2 Gt/year, which stems primarily from the combustion of fossil fuels and the effect of deforestation. Since industrialization, the ocean carbon reservoir has mitigated a substantial fraction of the increase of atmospheric CO_2. Estimates for the 1990s are that the ocean has taken up 118 Gt of the 244 Gt carbon emitted to the atmosphere by fossil fuel combustion (Denman et al., 2007), that is, today over half of the cumulative emissions are in the ocean. While this storage of anthropogenic carbon in the ocean prevents the associated radiative forcing and resulting warming in the atmosphere, it does have a measurable effect on the ocean's chemical status. The injection of CO_2 in the ocean increases the concentration of H^+-ions in the ocean because CO_2 reacts with H_2O to bicarbonate and a proton $\left(HCO_3^- + H^+\right)$. This makes the ocean more acidic, a process that is referred to as *ocean acidification*, and which is a direct effect of the increase of CO_2 concentrations in the atmosphere (Orr et al., 2005). The decrease of the ocean surface pH, a measure of the concentrations of H^+-ions: $pH = -\log_{10}(H^+)$, is well observed and amounts to about 0.1 pH-units since industrialization, that is, already 25% increase of the H^+-ion concentration has occurred (Feely et al., 2004). In the future, these changes are expected to increase significantly: depending on the

emissions of CO_2, further acidification and reductions in the pH of 0.14–0.35 are projected (Orr et al., 2005), which will result in a 50% reduction of the carbonate ion CO_3^{2-}.

A more acid ocean has thus a significantly reduced CO_3^{2-} concentration and therefore, the volume of ocean in which $CaCO_3$, that is mainly shells of marine calcifying organisms, dissolves, becomes larger (Joos et al., 2011). Simulations with coupled climate–carbon cycle models demonstrate that annual-mean undersaturation is imminent in the Arctic Ocean by about 2030, to be followed by the Southern Ocean by about 2050 for high emission scenarios (Steinacher et al., 2009). These model simulations further suggest that undersaturation in the Arctic is reached during at least one month already at an atmospheric CO_2 concentration of 409 ppm, which is expected to be reached before 2020. Of great concern is this change in chemical status of the world ocean for marine calcifying organisms such as corals and plankton as it may become more difficult for them to maintain their calcareous skeletons in an increasingly corrosive environment (Hoegh-Guldberg et al., 2007; Hoegh-Guldberg and Bruno, 2010).

8. CONCLUDING THOUGHTS

The ocean is a vast reservoir of water, energy, carbon, and many other substances, and due to its large surface interacting with the atmosphere, it represents a key component in the Earth System. Human activities since the industrial revolution have caused a massive increase of the concentrations of the major greenhouse gases to levels unprecedented in the past 800,000 years. This increase has warmed the atmosphere and led to many changes worldwide. Such changes are now unequivocally observed in the climate system (IPCC, 2007, 2013). These include continuous melting of the large ice sheets of Greenland and Antarctica (Shepherd et al., 2012), Arctic sea ice retreat and global-scale ocean warming from the surface downward. The increased CO_2 concentration in the atmosphere also increases the ocean's acidity with potentially adverse effects on marine ecosystems (Chapter 31). Were it not for the ocean's ability to absorb substantial amounts of heat and carbon, the effects of worldwide anthropogenic climate change would be much larger. The ocean is therefore already an important mitigating element in the Earth System. Future research will show to what extent we can continue to rely on the mitigation power of the world ocean. We know already now that the uptake capacity of the ocean for carbon will decrease due to a shift in the chemical composition of the ocean's surface and the uptake efficiency of heat due to the increased stratification and reduced vertical mixing that can be anticipated in an ocean that warms from the surface.

The combination of paleoclimatic reconstructions from many sites, and the spatial correlation among them, reveals that the ocean has played an active role in climate history. In contrast to the ocean being merely a passive reservoir, the sequence of abrupt climate changes observed during the past ice ages suggests that the ocean has only limited stability to perturbations. Simulations indicate that the ocean's overturning circulation may undergo transitions to fundamentally different equilibrium states for sufficiently large perturbations. Bifurcation points initiating such irreversible paths may be closer than our current knowledge suggests.

While the understanding of the ocean, its internal processes and its interactions with the other components of the Earth System remain patchy and incomplete, the strong concern emerges that the world ocean, and the global web of ecosystems embedded in it, may be more vulnerable to human impact than ever assumed. For responsible stewardship of this planet, we therefore urgently need the implementation of the scientific knowledge into tangible and forward-looking decisions. This is the crucial contribution of science to international negotiations that aim to implement Article 2[3] of the United Nations Framework Convention on Climate Change (UNFCCC, 1992) with the goal to limit anthropogenic climate change (UNFCCC, 2010). This requires global mitigation efforts, which must be established without delay (Stocker, 2013), and in a sufficiently comprehensive manner (Steinacher et al., 2013), if global mean warming and related consequences on the Earth System, and in particular on the world ocean, are to be limited.

ACKNOWLEDGMENTS

I thank Beat Ihly for designing Figures 1.2 and 1.3, and redrawing Figures 1.4 and 1.5, and Paul Durack, Aixue Hu, and Lynne Talley for contributing figures, and John A. Church, Peter Gent, Beat Ihly, Kevin Trenberth, Christoph Raible, and two anonymous reviewers for thoughtful reviews. The efficient editorial work by John A. Church and Gerold Siedler is appreciated.

REFERENCES

Abram, N.J., Gagan, M.K., Liu, Z., Hantoro, W.S., McCulloch, M.T., Suwargadi, B.W., 2007. Seasonal characteristics of the Indian Ocean Dipole during the Holocene epoch. Nature 445, 299–302.

Adkins, J.F., McIntyre, K., Schrag, D.P., 2002. The salinity, temperature, and $\delta^{18}O$ of the glacial deep ocean. Science 298, 1769–1773.

Alley, R.B., et al., 2003. Abrupt climate change. Science 299, 2005–2010.

Antonov, J.I., Levitus, S., Boyer, T.P., 2004. Climatological annual cycle of ocean heat content. Geophys. Res. Lett. 31, L04304.

Bamber, J.L., Riva, R.E.M., Vermeersen, B.L.A., LeBrocq, A.M., 2009. Reassessment of the potential sea-level rise from a collapse of the West Antarctic Ice Sheet. Science 324, 901–903.

3. UNFCCC Article 2: The ultimate objective of this Convention [. . .] is to achieve [. . .] stabilization of greenhouse gas concentrations in the atmosphere at a level that would prevent dangerous anthropogenic interference with the climate system. [. . .]

Barker, S., Diz, P., Vautravers, M.J., Pike, J., Knorr, G., Hall, I.R., Broecker, W.S., 2009. Interhemispheric Atlantic seesaw response during the last deglaciation. Nature 457, 1097–1103.

Barker, S., Knorr, G., Edwards, R.L., Parrenin, F., Putnam, A.E., Skinner, L.C., Wolff, E., Ziegler, M., 2011. 800,000 years of abrupt climate variability. Science 334, 347–351.

Becker, J.J., et al., 2009. Global bathymetry and elevation data at 30 arc seconds resolution: SRTM30_PLUS. Mar. Geod. 32, 355–371.

Bessières, L., Madec, G., Lyard, F., 2008. Global tidal residual mean circulation: does it affect a climate OGCM? Geophys. Res. Lett. 35, L03609.

Bindoff, N.L., et al., 2007. Observations: oceanic climate change and sea level. In: Solomon, S. et al., (Eds.), Climate Change 2007: The Physical Science Basis. Contribution of Working Group I to the Fourth Assessment Report of the Intergovernmental Panel on Climate Change. Cambridge University Press, Cambridge, pp. 385–432.

Bindoff, N.L., et al., 2013. Detection and attribution of climate change: from global to regional. In: Stocker, T.F. et al., (Eds.), Climate Change 2013: The Physical Science Basis. Contribution of Working Group I to the Fifth Assessment Report of the Intergovernmental Panel on Climate Change. Cambridge University Press, Cambridge.

Bjerknes, J., 1969. Atmospheric teleconnections from the equatorial Pacific. Mon. Weather Rev. 97, 163–172.

Blunier, T., et al., 1998. Asynchrony of Antarctic and Greenland climate change during the last glacial period. Nature 394, 739–743.

Braconnot, P., Harrison, S.P., Kageyama, M., Bartlein, P.J., Masson-Delmotte, V., Abe-Ouchi, A., Otto-Bliesner, B., Zhao, Y., 2012. Evaluation of climate models using palaeoclimatic data. Nat. Clim. Chang. 2, 417–424.

Broecker, W.S., 1987a. Unpleasant surprises in the greenhouse? Nature 328, 123–126.

Broecker, W.S., 1987b. The biggest chill. Nat. Hist. 96, 74–82.

Broecker, W.S., 1998. Paleocean circulation during the last deglaciation: a bipolar seesaw? Paleoceanography 13, 119–121.

Broecker, W.S., Denton, G.H., 1989. The role of ocean-atmosphere reorganizations in glacial cycles. Geochim. Cosmochim. Acta 53, 2465–2501.

Broecker, W.S., Peng, T.-H., 1982. Tracers in the Sea. Eldigio Press, Palisades, New York.

Brönnimann, S., 2007. Impact of El Niño-Southern Oscillation on European climate. Rev. Geophys. 45, RG3003.

Bryan, F., 1986. High-latitude salinity effects and interhemispheric thermohaline circulations. Nature 323, 301–304.

Cane, M.A., 2005. The evolution of El Niño, past and future. Earth Planet. Sci. Lett. 230, 227–240.

Capron, E., et al., 2010. Millennial and sub-millennial scale climatic variations recorded in polar ice cores over the last glacial period. Clim. Past 6, 345–365.

Cazenave, A., Llovel, W., 2010. Contemporary sea level rise. Ann. Rev. Mar. Sci. 2, 145–173.

Church, J.A., et al., 2011. Revisiting the Earth's sea-level and energy budgets from 1961 to 2008. Geophys. Res. Lett. 38, L18601.

Church, J.A., et al., 2013. Sea level change. In: Stocker, T.F. et al., (Eds.), Climate Change 2013: The Physical Science Basis. Contribution of Working Group I to the Fifth Assessment Report of the Intergovernmental Panel on Climate Change. Cambridge University Press, Cambridge.

Ciais, P., et al., 2013. Carbon and other biogeochemical cycles. In: Stocker, T.F. et al., (Eds.), Climate Change 2013: The Physical Science Basis. Contribution of Working Group I to the Fifth Assessment Report of the Intergovernmental Panel on Climate Change. Cambridge University Press, Cambridge.

Clark, P.U., Pisias, N.G., Stocker, T.F., Weaver, A.J., 2002. The role of the thermohaline circulation in abrupt climate change. Nature 415, 863–869.

Clark, P.U., Dyke, A.S., Shakun, J.D., Carlson, A.E., Clark, J., Wohlfarth, B., Mitrovica, J.X., Hostetler, S.W., McCabe, A.M., 2009. The last glacial maximum. Science 325, 710–714.

Clement, A.C., Peterson, L.C., 2008. Mechanisms of abrupt climate change of the last glacial period. Rev. Geophys. 46, RG4002.

Cobb, K.M., Charles, C.D., Cheng, H., Edwards, L., 2003. El Niño/Southern Oscillation and tropical Pacific climate during the last millennium. Nature 424, 271–276.

Cobb, K.M., Westphal, N., Sayani, H.R., Watson, J.T., Di Lorenzo, E., Cheng, H., Edwards, R.L., Charles, C.D., 2013. Highly variable El Niño–Southern oscillation throughout the Holocene. Science 339, 67–70.

Collins, M., et al., 2010. The impact of global warming on the tropical Pacific Ocean and El Niño. Nat. Geosci. 3, 391–397.

Collins, M., et al., 2013. Long-term climate change: projections, commitments and irreversibility. In: Stocker, T.F. et al., (Eds.), Climate Change 2013: The Physical Science Basis. Contribution of Working Group I to the Fifth Assessment Report of the Intergovernmental Panel on Climate Change. Cambridge University Press, Cambridge.

Crowley, T.J., 1992. North Atlantic deep water cools the southern hemisphere. Paleoceanography 7, 489–497.

Crutzen, P.J., Stoermer, E.F., 2000. The "Anthropocene" IGBP Newslett. 41, 17–18.

Cunningham, S.A., Alderson, S.G., King, B.A., Brandon, M.A., 2003. Transport and variability of the Antarctic Circumpolar Current in Drake Passage. J. Geophys. Res. 108, 8084.

Dansgaard, W., Johnsen, S.J., Clausen, H.B., Dahl-Jensen, D., Gundestrup, N., Hammer, C.U., Oeschger, H., 1984. North Atlantic climatic oscillations revealed by deep Greenland ice cores. In: Hansen, J.E., Takahashi, T. (Eds.), Climate Processes and Climate Sensitivity, vol. 29. American Geophysical Union, Washington, pp. 288–298.

Day, J.J., Hargreaves, J.C., Annann, J.D., Abe-Ouchi, A., 2012. Sources of multi-decadal variability in Arctic sea ice extent. Environ. Res. Lett. 7, 034011.

Defant, A., 1941. Quantitative Untersuchungen zu Statik und Dynamik des Atlantischen Ozeans: Die absolute Topographie des physikalischen Meeresniveaus und der Druckflächen sowie die Wasserbewegungen im Raum des Atlantischen Ozeans. Wissenschaftliche Ergebnisse der Deutschen Atlantischen Expedition auf dem Forschungs-und Vermessungsschiff "Meteor" 1925-1927, vol. 6. Walter de Gruyter, Berlin, pp. 191–260.

Delworth, T., Manabe, S., Stouffer, R.J., 1993. Interdecadal variations of the thermohaline circulation in a coupled ocean-atmosphere model. J. Clim. 6, 1993–2011.

Denman, K.L., et al., 2007. Couplings between changes in the climate system and biogeochemistry. In: Solomon, S. et al., (Eds.), Climate Change 2007: The Physical Science Basis. Contribution of Working Group I to the Fourth Assessment Report of the Intergovernmental Panel on Climate Change. Cambridge University Press, Cambridge, pp. 499–587.

Deser, C., Phillips, A.S., Hurrell, J.W., 2004. Pacific interdecadal climate variability: linkages between the Tropics and North Pacific during boreal winter since 1900. J. Clim. 17, 3109–3124.

Deser, C., Alexander, M.A., Xie, S.-P., Phillips, A.S., 2010. Sea surface temperature variability: patterns and mechanisms. Ann. Rev. Mar. Sci. 2, 115–143.

Döös, K., Nilsson, J., Nycander, J., Brodeau, L., Ballarotta, M., 2012. The world ocean thermohaline circulation. J. Phys. Oceanogr. 42, 1445–1460.

Durack, P.J., Wijffels, S.E., 2010. Fifty-year trends in global ocean salinities and their relationship to broad-scale warming. J. Clim. 23, 4342–4362.

Durack, P.J., Wijffels, S.E., Matear, R.J., 2012. Ocean salinities reveal strong global water cycle intensification during 1950 to 2000. Science 336, 455–458.

Dutton, A., Lambeck, K., 2012. Ice volume and sea level during the last interglacial. Science 337, 216–219.

EPICA Community Members, 2006. One-to-one coupling of glacial climate variability in Greenland and Antarctica. Nature 444, 195–198.

Fasullo, J.T., Trenberth, K.E., 2008. The annual cycle of the energy budget. Part I: global mean and land-ocean exchanges. J. Clim. 21, 2297–2312.

Feely, R.A., Sabine, C.L., Lee, K., Berelson, W., Kleypas, J., Fabry, V.J., Millero, F.J., 2004. Impact of anthropogenic CO_2 on the $CaCO_3$ system in the oceans. Science 305, 362–366.

Ferrari, R., Wunsch, C., 2009. Ocean circulation kinetic energy: reservoirs, sources, and sinks. Annu. Rev. Fluid Mech. 41, 253–282.

Ferrari, R., Wunsch, C., 2010. The distribution of eddy kinetic and potential energies in the global ocean. Tellus 62A, 92–108.

Ferreira, D., Marshall, J., Rose, B., 2011. Climate determinism revisited: multiple equilibria in a complex climate model. J. Clim. 24, 992–1012.

Fischer, H., et al., 2010. The role of Southern Ocean processes in orbital and millennial CO_2 variations—a synthesis. Quat. Sci. Rev. 29, 193–205.

Fleitmann, D., et al., 2009. Timing and climatic impact of Greenland interstadials recorded in stalagmites from northern Turkey. Geophys. Res. Lett. 36, L19707.

Ganachaud, A., Wunsch, C., 2000. Improved estimates of global ocean circulation, heat transport and mixing from hydrographic data. Nature 408, 453–457.

Ganachaud, A., Wunsch, C., 2003. Large-scale ocean heat and freshwater transports during the World Ocean Circulation Experiment. J. Clim. 16, 696–705.

Gebbie, G., Huybers, P., 2012. The mean age of ocean waters inferred from radiocarbon observations: sensitivity to surface sources and accounting for mixing histories. J. Phys. Oceanogr. 42, 291–305.

Gleckler, P.J., et al., 2012. Human-induced global ocean warming on multidecadal timescales. Nat. Clim. Chang. 2, 524–529.

Gordon, A., 1991. The Role of Thermohaline Circulation in Global Climate Change. Lamont–Doherty Geological Observatory of Columbia University, Palisades, New York, pp. 44–51.

Gray, S.T., Graumlich, L.J., Betancourt, J.L., Pederson, G.T., 2004. A tree-ring based reconstruction of the Atlantic Multidecadal Oscillation since 1567 A.D. Geophys. Res. Lett. 31, L12205.

Gregory, J.M., Huybrechts, P., 2006. Ice-sheet contributions to future sea-level change. Philos. Trans. R. Soc. A 364, 1709–1731.

Guilyardi, E., Wittenberg, A., Fedorov, A., Collins, M., Wang, C., Capotondi, A., van Oldenborgh, G.J., Stockdale, T., 2009. Understanding El Niño in ocean-atmosphere general circulation models. Bull. Am. Meteorol. Soc. 90, 325–340.

Halpert, M.S., Ropelewski, C.F., 1992. Surface temperature patterns associated with the southern oscillation. J. Clim. 5, 577–593.

Held, I.M., Soden, B.J., 2006. Robust responses of the hydrological cycle to global warming. J. Clim. 19, 5686–5699.

Hoegh-Guldberg, O., Bruno, J.F., 2010. The impact of climate change on the world's marine ecosystems. Science 328, 1523–1528.

Hoegh-Guldberg, O., et al., 2007. Coral reefs under rapid climate change and ocean acidification. Science 318, 1737–1742.

Holland, D.M., Thomas, R.H., De Young, B., Ribbergaard, M.H., Lyberth, B., 2008. Acceleration of Jakobshavn Isbræ triggered by warm subsurface ocean waters. Nat. Geosci. 1, 659–664.

Hu, A., et al., 2012. Role of the Bering Strait on the hysteresis of the ocean conveyor belt circulation and glacial climate stability. Proc. Natl. Acad. Sci. U.S.A. 109, 6417–6422.

Huang, R.X., 2010. Ocean Circulation. Cambridge University Press, Cambridge, 791 pp.

Huber, C., Leuenberger, M., Spahni, R., Flückiger, J., Schwander, J., Stocker, T.F., Johnsen, S., Landais, A., Jouzel, J., 2006. Isotope calibrated Greenland temperature record over Marine Isotope Stage 3 and its relation to CH_4. Earth Planet. Sci. Lett. 243, 504–519.

Hurlburt, H.E., et al., 2009. High-resolution global and basin-scale ocean analyses and forecasts. Oceanography 22, 110–127.

Imawaki, S., Uchida, H., Ichikawa, H., Fukasawa, M., Umatani, S., ASUKA Group, 2001. Satellite altimeter monitoring the Kurosio transport south of Japan. Geophys. Res. Lett. 28, 17–20.

IPCC, 2007. Climate Change 2007: Solomon, S. et al., (Eds.), The Physical Science Basis. Contribution of Working Group I to the Fourth Assessment Report of the Intergovernmental Panel on Climate Change. Cambridge University Press, Cambridge.

IPCC, 2013. Climate Change 2013: The Physical Science Basis. In: Stocker, T.F. et al., (Eds.), Contribution of Working Group I to the Fifth Assessment Report of the Intergovernmental Panel on Climate Change. Cambridge University Press, Cambridge.

Izumo, T., Vialard, J., Lengaigne, M., de Boyer Montegut, C., Behera, S.K., Luo, J.-J., Cravatte, S., Masson, S., Yamagata, T., 2010. Influence of the state of the Indian Ocean Dipole on the following year's El Niño. Nat. Geosci. 3, 168–172.

Jansen, E., et al., 2007. Paleoclimate. In: Solomon, S. et al., (Eds.), Climate Change 2007: The Physical Science Basis. Contribution of Working Group I to the Fourth Assessment Report of the Intergovernmental Panel on Climate Change. Cambridge University Press, Cambridge, pp. 433–497.

Johns, W.E., et al., 2011. Continuous, array-based estimates of Atlantic Ocean heat transport at 26.58°N. J. Clim. 24, 2429–2449.

Joos, F., Frölicher, T.L., Steinacher, M., Plattner, G.-K., 2011. Impact of climate change mitigation on ocean acidification projections. In: Gattuso, J.-P., Hansson, L. (Eds.), Ocean Acidification. Oxford University Press, Oxford, pp. 272–290.

Joughin, I., Alley, R.B., 2011. Stability of the West Antarctic ice sheet in a warming world. Nat. Geosci. 4, 506–513.

Kavvada, A., Ruiz-Barradas, A., Nigam, S., 2013. AMO's structure and climate footprint in observations and IPCC AR5 climate simulations. Clim. Dyn. http://dx.doi.org/10.1007/s00382-013-1712-1.

Kohfeld, K.E., Ridgwell, A., 2009. Glacial-interglacial variability in atmospheric CO_2. In: Le Quéré, C., Saltzman, E.S. (Eds.), Surface Ocean—Lower Atmosphere Processes, vol. 187. American Geophysical Union, Washington, pp. 251–286.

Koltermann, K.P., Gouretski, V.V., Jancke, K., 2011. Hydrographic Atlas of the World Ocean Circulation Experiment (WOCE). In: Sparrow, M. et al., (Eds.), Atlantic Ocean, vol. 3. International WOCE Project Office, Southampton, UK.

Labat, D., Goddéris, Y., Probst, J.L., Guyot, J.L., 2004. Evidence for global runoff increase related to climate warming. Adv. Water Res. 27, 631–642.

Large, W.G., Yeager, S.G., 2009. The global climatology of an interannually varying air-sea flux data set. Clim. Dyn. 33, 341–364.

Levitus, S., Burgett, R., Boyer, T.P., 1994. In: NOAA Atlas NESDIS 3, World Ocean Atlas 1994. Salinity, vol. 3. NOAA, U.S. Department of Commerce.

Levitus, S., et al., 2012. World ocean heat content and thermosteric sea level change (0−2000 m), 1955−2010. Geophys. Res. Lett. 39, L10603.

Li, T., Wang, B., Chang, C.-P., Zhang, Y., 2003. A theory for the Indian Ocean Dipole-Zonal Mode. J. Atmos. Sci. 60, 2119–2135.

Liu, Z., 2012. Dynamics of interdecadal climate variability: a historical perspective. J. Clim. 25, 1963–1995.

Liu, Z., Alexander, M., 2007. Atmospheric bridge, oceanic tunnel, and global climatic teleconnections. Rev. Geophys. 45, RG2005.

Lumpkin, R., Speer, K., 2003. Large-scale vertical and horizontal circulation in the North Atlantic Ocean. J. Phys. Oceanogr. 33, 1902–1920.

Lund, D.C., Adkins, J.F., Ferrari, R., 2011. Abyssal Atlantic circulation during the Last Glacial Maximum: constraining the ratio between transport and vertical mixing. Paleoceanography 26, PA1213.

Luo, J.-J., Zhang, R., Behera, S.K., Masumoto, Y., Jin, F.-F., Lukas, R., Yamagata, T., 2010. Interaction between El Niño and extreme Indian Ocean Dipole. J. Clim. 23, 726–742.

Lüthi, D., et al., 2008. High-resolution carbon dioxide concentration record 650,000-800,000 years before present. Nature 453, 379–382.

Lyman, J.M., Good, S.A., Gouretski, V.V., Ishii, M., Johnson, G.C., Palmer, M.D., Smith, D.M., Willis, J.K., 2010. Robust warming of the global upper ocean. Nature 465, 334–337.

Lynch-Stieglitz, J., 2003. Tracers of past ocean circulation. In: Holland, H.D., Turekian, K.K. (Eds.), Treatise on Geochemistry, vol. 6. Elsevier, Amsterdam, pp. 433–451.

Lynch-Stieglitz, J., et al., 2007. Atlantic meridional overturning circulation during the Last Glacial Maximum. Science 316, 66–69.

MacDonald, G.M., Case, R.A., 2005. Variations in the Pacific Decadal Oscillation over the past millennium. Geophys. Res. Lett. 32, L08703.

Maltrud, M.E., McClean, J.L., 2005. An eddy resolving global 1/10° ocean simulation. Ocean Model. 8, 31–54.

Manabe, S., Stouffer, R.J., 1988. Two stable equilibria of a coupled ocean atmosphere model. J. Clim. 1, 841–866.

Manabe, S., Stouffer, R.J., 1993. Century-scale effects of increased atmospheric CO_2 on the ocean-atmosphere system. Nature 364, 215–218.

Manabe, S., Stouffer, R.J., 1994. Multiple-century response of a coupled ocean-atmosphere model to an increase of atmospheric carbon dioxide. J. Clim. 7, 5–23.

Mantua, N.J., Hare, S.R., 2002. The Pacific Decadal Oscillation. J. Oceanogr. 58, 35–44.

Marchal, O., Curry, W.B., 2008. On the abyssal circulation in the glacial Atlantic. J. Phys. Oceanogr. 38, 2014–2037.

MARGO Project Members, 2009. Constraints on the magnitude and patterns of ocean cooling at the Last Glacial Maximum. Nat. Geosci. 2, 127–132.

Marshall, J., Speer, K., 2012. Closure of the meridional overturning circulation through Southern Ocean upwelling. Nat. Geosci. 5, 171–180.

Masson-Delmotte, V., et al., 2013. Information from Paleoclimate Archives. In: Stocker, T.F. et al., (Eds.), Climate Change 2013: The Physical Science Basis. Contribution of Working Group I to the Fifth Assessment Report of the Intergovernmental Panel on Climate Change. Cambridge University Press, Cambridge.

Meehl, G.A., et al., 2007. Global Climate Projections. In: Solomon, S. et al., (Eds.), Climate Change 2007: The Physical Science Basis. Contribution of Working Group I to Fourth Assessment Report of the Intergovernmental Panel on Climate Change. Cambridge University Press, Cambridge, pp. 747–845.

Meehl, G.A., et al., 2012. Climate system response to external forcings and climate change projections in CCSM4. J. Clim. 25, 3661–3683.

Menviel, L., Joos, F., Ritz, S.P., 2012. Simulating atmospheric CO_2, ^{13}C and the marine carbon cycle during the Last Glacial-Interglacial cycle: possible role for a deepening of the mean remineralization depth and an increase in the oceanic nutrient inventory. Quat. Sci. Rev. 56, 46–68.

Mikolajewicz, U., Gröger, M., Maier-Reimer, E., Schurgers, G., Vizcaino, M., Winguth, A.M.E., 2007. Long-term effects of anthropogenic CO_2 emissions simulated with a complex earth system model. Clim. Dyn. 28, 599–633.

Mölg, T., Renold, M., Vuille, M., Cullen, N.J., Stocker, T.F., Kaser, G., 2006. Indian Ocean Zonal Mode activity in a multicentury-integration of a coupled AOGCM consistent with climate proxy data. Geophys. Res. Lett. 33, L18710.

Moss, R.H., et al., 2010. The next generation of scenarios for climate change research and assessment. Nature 463, 747–756.

Munk, W., 1966. Abyssal recipes. Deep Sea Res. 13, 707–730.

Munk, W., Wunsch, C., 1998. Abyssal recipes II, energetics of tidal and wind mixing. Deep Sea Res. 45, 1977–2010.

North Greenland Ice Core Project members, 2004. High-resolution climate record of the northern hemisphere back into the last interglacial period. Nature 431, 147–151.

Oeschger, H., Beer, J., Siegenthaler, U., Stauffer, B., Dansgaard, W., Langway, C.C., 1984. Late glacial climate history from ice cores. In: Hansen, J.E., Takahashi, T. (Eds.), Climate Processes and Climate Sensitivity, vol. 29. American Geophysical Union, Washington, pp. 299–306.

Oka, A., Hasumi, H., Abe-Ouchi, A., 2012. The thermal threshold of the Atlantic meridional overturning circulation and its control by wind stress forcing during glacial climate. Geophys. Res. Lett. 39, L09709.

Oort, A.H., Anderson, L.A., Peixoto, J.P., 1994. Estimates of the energy cycle of the oceans. J. Geophys. Res. 99, 7665–7688.

Orr, J.C., et al., 2005. Anthropogenic ocean acidification over the twenty-first century and its impact on calcifying organisms. Nature 437, 681–686.

Otto-Bliesner, B.L., Hewitt, C.D., Marchitto, T.M., Brady, E., Abe-Ouchi, A., Crucifix, M., Murakami, S., Weber, S.L., 2007. Last Glacial Maximum ocean thermohaline circulation: PMIP2 model intercomparisons and data constraints. Geophys. Res. Lett. 34, L12706.

Ou, H.-W., 2012. A minimal model of the Atlantic multidecadal variability: its genesis and predictability. Clim. Dyn. 38, 775–794.

Peixoto, J.P., Oort, A.H., 1992. Physics of Climate. American Institute of Physics, New York, USA, 520 pp.

Pierrehumbert, R.T., Abbot, D.S., Voigt, A., Koll, D., 2011. Climate of the Neoproterozoic. Annu. Rev. Earth Planet. Sci. 39, 417–460.

Piotrowski, A.M., Goldstein, S.L., Hemming, S.R., Fairbanks, R.G., 2004. Intensification and variability of ocean thermohaline circulation through the last deglaciation. Earth Planet. Sci. Lett. 225, 205–220.

Plattner, G.-K., et al., 2008. Long-term climate commitments projected with climate—carbon cycle models. J. Clim. 21, 2721–2751.

Purkey, S.G., Johnson, G.C., 2010. Warming of global abyssal and deep Southern Ocean Waters between the 1990s and 2000s: contributions to global heat and sea level rise budgets. J. Clim. 23, 6336–6351.

Rahmstorf, S., et al., 2005. Thermohaline circulation hysteresis: a model intercomparison. Geophys. Res. Lett. 32, L23605.

Rein, B., Lückge, A., Reinhardt, L., Sirocko, F., Wolf, A., Dullo, W.-C., 2005. El Niño variability off Peru during the last 20,000 years. Paleoceanography 20, PA4003.

Rempfer, J., Stocker, T.F., Joos, F., Dutay, J.-C., Siddall, M., 2011. Modelling isotopes of neodymium with a coarse resolution ocean circulation model: sensitivities to model parameters and source/sink distributions. Geochim. Cosmochim. Acta 75, 5927–5950.

Rempfer, J., Stocker, T.F., Joos, F., Dutay, J.-C., 2012. On the relationship between Nd isotopic composition and ocean overturning circulation in idealized freshwater discharge events. Paleoceanography 27, PA3211.

Rhein, M., et al., 2013. Observations: Ocean. In: Stocker, T.F. et al., (Eds.), Climate Change 2013: The Physical Science Basis. Contribution of Working Group I to the Fifth Assessment Report of the Intergovernmental Panel on Climate Change. Cambridge University Press, Cambridge.

Richardson, P.L., 2008. On the history of meridional overturning circulation schematic diagrams. Prog. Oceanogr. 76, 466–486.

Risien, C.M., Chelton, D.B., 2008. A global climatology of surface wind and wind stress fields from eight years of QuikSCAT scatterometer data. J. Phys. Oceanogr. 38, 2379–2413.

Ritz, S.P., Stocker, T.F., Grimalt, J.O., Menviel, L., Timmermann, A., 2013. Estimated strength of the Atlantic overturning circulation during the last deglaciation. Nat. Geosci. 6, 208–212.

Riva, R.E.M., Bamber, J.L., Lavallé, D.A., Wouters, B., 2010. Sea-level fingerprint of continental water and ice mass change from GRACE. Geophys. Res. Lett. 37, L19605.

Robinson, A., Calov, R., Ganopolski, A., 2012. Multistability and critical thresholds of the Greenland ice sheet. Nat. Clim. Chang. 2, 429–432.

Roemmich, D., Gilson, J., 2009. The 2004–2008 mean and annual cycle of temperature, salinity, and steric height in the global ocean from the Argo Program. Prog. Oceanogr. 82, 81–100.

Ropelewski, C.F., Halpert, M.S., 1987. Global and regional scale precipitation patterns associated with the El Niño/Southern Oscillation. Mon. Weather Rev. 115, 1606–1626.

Saji, N.H., Goswami, B.N., Vinayachandran, P.N., Yamagata, T., 1999. A dipole mode in the tropical Indian Ocean. Nature 401, 360–363.

Sarachik, E.S., Cane, M.A., 2010. The El Niño-Southern Oscillation Phenomenon. In: Cambridge University Press, Cambridge, 369 pp.

Schäfer-Neth, C., Paul, A., 2003. The Atlantic Ocean at the last glacial maximum: 1. Objective mapping of the GLAMAP sea-surface conditions. In: Wefer, G. et al., (Eds.), The South Atlantic in the Late Quaternary: Material Budget and Current Systems. Springer, Berlin, pp. 531–548.

Schlesinger, M.E., Ramankutty, N., 1994. An oscillation in the global climate system of period 65-70 years. Nature 367, 723–726.

Schmitz, W.J., 1996. On the world ocean circulation: Volume II. The Pacific and Indian Oceans/A global update. Technical Report WHOI-96-08, Woods Hole Oceanographic Institution, 237 pp.

Schott, F.A., Xie, S.-P., McCreary Jr., J.P., 2009. Indian ocean circulation and climate variability. Rev. Geophys. 47, RG1002.

Shen, C., Wang, W.-C., Gong, W., Hao, Z., 2006. A Pacific Decadal Oscillation record since 1470 AD reconstructed from proxy data of summer rainfall over eastern China. Geophys. Res. Lett. 33, L03702.

Shepherd, A., et al., 2012. A reconciled estimate of ice-sheet mass balance. Science 338, 1183–1189.

Siddall, M., Stocker, T.F., Blunier, T., Spahni, R., McManus, J., Bard, E., 2006. Using a maximum simplicity paleoclimate model to simulate millennial variability during the last four glacial periods. Quat. Sci. Rev. 25, 3185–3197.

Siegenthaler, U., et al., 2005. Stable carbon cycle-climate relationship during the Late Pleistocene. Science 310, 1313–1317.

Sigman, D.M., Boyle, E.A., 2000. Glacial/interglacial variations in atmospheric carbon dioxide. Nature 407, 859–869.

Steffensen, J.P., et al., 2008. High-resolution Greenland ice core data show abrupt climate change happens in few years. Science 321, 680–684.

Steinacher, M., Joos, F., Frölicher, T.L., Plattner, G.-K., Doney, S.C., 2009. Imminent ocean acidification in the Arctic projected with the NCAR global coupled carbon cycle-climate model. Biogeosciences 6, 515–533.

Steinacher, M., Joos, F., Stocker, T.F., 2013. Allowable carbon emissions lowered by multiple climate targets. Nature 499, 197–201.

Stenni, B., et al., 2011. Expression of the bipolar see-saw in Antarctic climate records during the last deglaciation. Nat. Geosci. 4, 46–49.

Stephens, G.L., et al., 2012. An update on Earth's energy balance in light of the latest global observations. Nat. Geosci. 5, 691–696.

Stevenson, S.L., 2012. Significant changes to ENSO strength and impacts in the twenty-first century: results from CMIP5. Geophys. Res. Lett. 39, L17703.

Stocker, T.F., 1998. The seesaw effect. Science 282, 61–62.

Stocker, T.F., 2000. Past and future reorganisations in the climate system. Quat. Sci. Rev. 19, 301–319.

Stocker, T.F., 2013. The closing door of climate targets. Science 339, 280–282.

Stocker, T.F., Johnsen, S.J., 2003. A minimum thermodynamic model for the bipolar seesaw. Paleoceanography 18, 1087.

Stocker, T.F., Marchal, O., 2000. Abrupt climate change in the computer: is it real? Proc. Natl. Acad. Sci. U.S.A. 97, 1362–1365.

Stocker, T.F., Schmittner, A., 1997. Influence of CO_2 emission rates on the stability of the thermohaline circulation. Nature 388, 862–865.

Stocker, T.F., Wright, D.G., 1991. Rapid transitions of the ocean's deep circulation induced by changes in surface water fluxes. Nature 351, 729–732.

Stocker, T.F., Wright, D.G., Mysak, L.A., 1992. A zonally averaged, coupled ocean-atmosphere model for paleoclimate studies. J. Clim. 5, 773–797.

Stommel, H., 1957. A survey of ocean current theory. Deep Sea Res. 4, 149–184.

Stommel, H., 1958. The abyssal circulation. Deep Sea Res. 5, 80–82.

Stommel, H., 1961. Thermohaline convection with two stable regimes of flow. Tellus 13, 224–230.

Stommel, H., Arons, A.B., 1960. On the abyssal circulation of the world ocean—I. Stationary planetary flow patterns on a sphere. Deep Sea Res. 6, 140–154.

Stott, P.A., Gillett, N.P., Hegerl, G.C., Karoly, D.J., Stone, D.A., Zhang, X., Zwiers, F., 2010. Detection and attribution of climate change: a regional perspective. Wiley Interdiscip. Rev. Clim. Change 1, 192–211.

Stouffer, R.J., Manabe, S., 2003. Equilibrium response of thermohaline circulation to large changes in atmospheric CO_2 concentration. Clim. Dyn. 20, 759–773.

Sutton, R.T., Hodson, D.L.R., 2003. Influence of the ocean on North Atlantic climate variability 1871-1999. J. Clim. 16, 3296–3313.

Takahashi, T., et al., 2009. Climatological mean and decadal change in surface ocean pCO_2, and net sea–air CO_2 flux over the global oceans. Deep Sea Res. II 56, 554–577.

Talley, L.D., 2003. Shallow, intermediate, and deep overturning components of the global heat budget. J. Phys. Oceanogr. 33, 530–560.

Talley, L.D., 2008. Freshwater transport estimates and the global overturning circulation: shallow, deep and throughflow components. Prog. Oceanogr. 78, 257–303.

Talley, L.D., 2013. Closure of the global overturning circulation through the Indian, Pacific and Southern Oceans: schematics and transports. Oceanography 26, 80–97.

Talley, L.D., Pickard, G.L., Emery, W.J., Swift, J.H., 2011. Descriptive Physical Oceanography. Elsevier, Amsterdam, 555 pp.

Timmermann, A., Oberhuber, J.M., Bacher, A., Esch, M., Latif, M., Roeckner, E., 1999. Increased El Niño frequency in a climate model forced by future greenhouse warming. Nature 398, 694–696.

Trenberth, K.E., Smith, L., Qian, T., Dai, A., Fasullo, J., 2007. Estimates of the global water budget and its annual cycle using observational and model data. J. Hydrometeorol. 8, 758–769.

Trenberth, K.E., Fasullo, J.T., Mackaro, J., 2011. Atmospheric moisture transports from ocean to land and global energy flows in reanalyses. J. Clim. 24, 4907–4924.

UNFCCC, 1992. United Nations Framework Convention on Climate Change (FCCC/INFORMAL/84 GE.05-62220 (E) 200705). United Nations, New York.

UNFCCC, 2010. The Cancun Agreements, FCCC/CP/2010/7/Add.1. United Nations Framework Convention on Climate Change.

Verschuuren, D., Laird, K.R., Cumming, B.F., 2000. Rainfall and drought in equatorial east Africa during the past 1,100 years. Nature 403, 410–414.

Voelker, A.H.L., Workshop-Participants, 2002. Global distribution of centennial-scale records for Marine Isotope Stage (MIS) 3: a database. Quat. Sci. Rev. 21, 1185–1212.

Wang, C., 2001. A unified oscillator model for the El Niño-Southern Oscillation. J. Clim. 14, 98–115.

Webster, P.J., Moore, A.M., Loschnigg, J.P., Leben, R.R., 1999. Coupled ocean-atmosphere dynamics in the Indian Ocean during 1997-98. Nature 401, 356–360.

Wijffels, S.E., 2001. Ocean transport of fresh water. In: Siedler, G. et al., (Eds.), Ocean Circulation & Climate: Observing and Modelling the Global Ocean. International Geophysics Series, vol. 77. Academic Press, pp. 475–488.

Wunsch, C., 1998. The work done by the wind on the oceanic general circulation. J. Phys. Oceanogr. 28, 2332–2340.

Wunsch, C., Ferrari, R., 2004. Vertical mixing, energy, and the general circulation of the oceans. Annu. Rev. Fluid Mech. 36, 281–314.

Xie, S.-P., Annamalai, H., Schott, F.A., McCreary, J.P., 2002. Structure and mechanisms of South Indian Ocean climate variability. J. Clim. 15, 864–878.

Zaucker, F., Broecker, W.S., 1992. The influence of atmospheric moisture transport on the fresh water balance of the Atlantic drainage basin: general circulation model simulations and observations. J. Geophys. Res. 97, 2765–2773.